2007

Mathematical Model of Ethanol Metabolism in Liver

Parag Pande
Cleveland State University

MATHEMATICAL MODEL OF ETHANOL METABOLISM IN LIVER

PARAG PANDE

Bachelor of Chemical Engineering

Pune University

August, 2001

Submitted in partial fulfillment of requirements for the degree

MASTER OF SCIENCE IN CHEMICAL ENGINEERING

at the

CLEVELAND STATE UNIVERSITY

DECEMBER 2007

This thesis has been approved

For the department of **CHEMICAL AND BIOMEDICAL ENGINEERING**.

and the College of Graduate Studies by

_____

Dr. Joanne M. Belovich, Thesis Committee Chairperson

Chemical and Biomedical Engineering. /_____

Department / Date

_____

Dr. Jorge E. Gatica, Thesis Committee Member

Chemical and Biomedical Engineering. /_____

Department / Date

_____

Dr. Sridhar Ungarala, Thesis Committee Member

Chemical and Biomedical Engineering. /_____

Department / Date

ACKNOWLEDGEMENT

First and foremost, I would like to thank Dr. Joanne Belovich for her consistent guidance and support throughout my research. Working with her has been a growing inspiration to contribute and excel. Her ever present guidance in matters of academic and beyond has been central in enriching my graduate school experience.

I would like to thank Dr Jorge Gatica for guiding with his exquisite knowledge and experience from time to time. I would like to thank Dr. Sridhar Ungarala for reviewing my thesis.

This research has been funded by NIH grant (NIGMS P50-GM-66309). I would like to express my gratitude towards our collaborators from Case Western Reserve University, Dr. Gerald Saidel, Dr. Richard Hanson, my coworker Elie Chalhoub and our department secretary Ms. Becky Laird for their help and support in completing my research work.

Finally, I would also like to thank my parents, who always believed in me and made it possible for me to pursue my graduate studies.

MATHEMATICAL MODEL OF ETHANOL METABOLISM IN LIVER

PARAG PANDE

ABSTRACT

A lumped mathematical model of liver metabolism is presented to analyze the effect of ethanol on metabolic processes of 24 hr fasted rats. The model is developed in two parts. In the first part individual kinetic models for important regulatory steps in the liver metabolic pathways are developed and in second part transport and mass balance equations in the two well mixed domains: tissue and blood, are developed to calculate intermediate metabolite concentrations and fluxes in response to the changes in ethanol and lactate concentrations in the perfusion medium. Part of the model without ethanol metabolism has been validated and published in Chalhoub et al, 2007. The focus of this effort was to illustrate the effect of ethanol metabolism on gluconeogenesis from lactate. The kinetic models developed for phosphofructokinase and fructose 1,6 bisphosphatase have been independently validated with data from the literature, whereas the results of the comprehensive lumped model are compared with the data from Krebs et al (1969). While the lumped model show many important characteristics of ethanol metabolism and predicts the flux of glucose production in the same range, two major contradictions of the simulated results with experimental data are observed. These shortcomings are discussed with appropriate reasoning. The model presented in this thesis is expected to improve the understanding on the effects of ethanol metabolism and provide a practical tool to address alcohol related health issues.

TABLE OF CONTENTS

LIST OF TABLES

LIST OF FIGURES

CHAPTER I

INTRODUCTION

The mathematical model developed here attempts to provide a useful research tool for understanding and predicting key characteristics of liver metabolism. The importance of this effort is apparent from advantages such as quantifying intermediate metabolite concentrations and fluxes in response to changes in various substrate concentrations.

Liver is one of the primary organs in vertebrates. The human liver is constructed of approximately one million lobules, which essentially are the basic functioning units. Each of these lobules consists of a hexagonal row of hepatic cells called hepatocytes. Two of the major functions of liver are carbohydrate metabolism to generate energy, and removal of toxic components by channeling them into metabolic pathways. This is achieved through the metabolic reactions that take place in hepatocytes, and are controlled with a very complex regulation through biological catalysts (enzymes). With over a thousand of such metabolic reactions, each depending on number characteristics like concentration of substrates and other metabolic intermediates and the activity of enzyme, developing a model that can describe the complete *in vivo* behavior of liver is a challenge.

Ethanol has a large number of physiological repercussions. Alcoholism has been reported as one of the leading cause for a number of health issues and diseases [35, 60,

61, 69]. Ethanol and its oxidation product acetaldehyde severely impair normal functions of hepatocytes causing hypoglycemia, and alcoholic liver diseases such as hepatitis, cirrhosis and fatty liver. Ethanol also affects other organs like brain, heart and kidney. The only way to eliminate ethanol by the body is to metabolize it in the liver [35, 60, 61, 62]. Thus a model of liver metabolism which can also account for the effects of ethanol metabolism can be of significant assistance to understand and treat diseases related to alcohol.

This work has been divided in three parts based on specific aims. The primary objective of our group was to develop a robust and realistic mathematical model considering the organ as a lumped system (well mixed), validate it with the available data in the literature to show its predictability, and confirm its usefulness by comparing the response of the model to addition of ethanol with data in the literature. For this endeavor important requisites were: sound understanding of intricate regulations of metabolic processes to develop individual kinetic expressions for each important regulatory step (which can allow us to grasp the *in vivo* characteristics in the comprehensive model), transport kinetics for each metabolite between blood and tissue, and the dynamic mass balances to predict the changes in concentrations and fluxes of metabolites with respect to time.

Consequently, the first part of the thesis develops the kinetic expression for phosphofructokinase and fructose 1,6-bisphosphatase, which catalyze two of the most important regulatory steps in the glycolytic and gluconeogenic pathways. The second part describes the selection of the kinetic expressions for alcohol and aldehyde dehydrogenase which are the ethanol metabolizing enzymes. The third part incorporates these kinetic

models along with the complementary expressions for transport into a lumped model which can account for the effects of ethanol metabolism.

In this work, the mechanistic kinetic expressions presented in the first two parts are the quantitative description of enzyme regulation and function, in different hormonal and nutritional states with high degree of generality. The lumped model developed with the help of these expressions, along with the transport kinetics and mass balances presents a promising tool for understanding and predicting fundamental processes in metabolic system. Finally the investigation of the effect of ethanol on gluconeogenesis demonstrates credibility of the model in physiological context. Successful comprehensive models to this level of detail have not been formulated to date, which makes this a distinguishing effort with a very worthwhile goal.

CHAPTER II

BACKGROUND

2.1 Mechanism of Ethanol Metabolism

Ethanol is an aliphatic (open chain) compound with low molecular weight. It is completely soluble in water via the formation of intermolecular hydrogen bonds with the hydroxyl groups of water. As a result of this complete solubility in water, ethanol can be readily distributed throughout the body, crossing important biological membranes, such as the blood brain barrier, to affect a large number of organs and biological processes [66]. Ethanol is not known to be formed in the mammalian body nor it is present in any of the natural food sources, therefore strong metabolic processes involving allosteric or back regulation (such as for lactate, glucose) are absent [37, 39].

Ethanol taken via oral ingestion passes through the esophagus into the stomach and small intestine, where it is absorbed into the bloodstream (approximately 20% from stomach and 80% from small intestine). A very small fraction of ethanol can be eliminated through lungs and kidneys. Since ethanol cannot be stored in the body, it must be metabolized to be eliminated. Alcohol can only be metabolized in the liver, where enzymes are found to initiate the process [36, 37, 45, 60]. Two pathways of ethanol

metabolism have been extensively studied in literature, (i) through the reactions catalyzed by alcohol dehydrogenase (ADH) and (ii) through the Microsomal Ethanol Oxidizing System (MEOS) [60, 61].

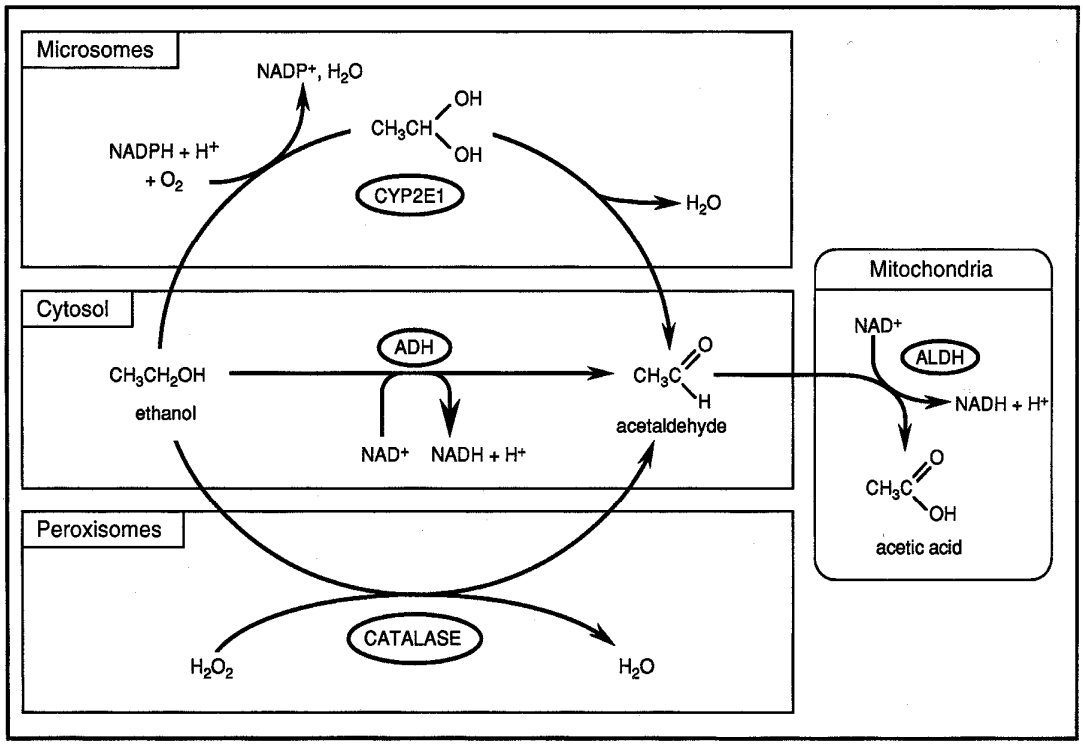

Figure 1. Possible metabolic pathways of ethanol metabolism [66].

A number of papers are published in the literature dealing with MEOS [60, 61, 62, 63, 64]. These papers can be divided in two groups: those where the ethanol oxidation is believed to occur due to the unique enzyme system involving Cytochrome P450 (CYP2E1)[61, 63], and those which support the findings that the predominant mechanism for ethanol metabolism is NADPH dependent hydrogen peroxide (H_2O_2) production (by the microsomal electron transport) followed by the peroxidation of alcohol to acetaldehyde by catalase[60, 62]. These mechanisms are shown in Figure 1. However,

whether any of these systems functions *in vivo* or only in perfused organs, and the extent of their contribution in total ethanol elimination is highly controversial. The MEOS system consisting either of Cytochrome P450 or catalase is not inhibited by pyrazole, which is a strong, competitive inhibitor of alcohol dehydrogenase. Inhibition studies of alcohol dehydrogenase show a negligible rate of ethanol removal in liver for *in vivo* conditions [36, 60, 61]. Also some of the findings strongly suggest that the generation of reducing equivalence from alcohol dehydrogenation inhibits H_2O_2 generation leading to significantly diminished rates of ethanol peroxidation via catalase [62]. Under the conditions of chronic and high dosage of ethanol, catalase may play a small role, but even under these circumstances the rate of removal of ethanol is very low as compared to that of alcohol dehydrogenase. The reaction catalyzed by alcohol dehydrogenase (ADH) is still considered the primary and most important pathway for ethanol metabolism. The scope of this thesis is limited to the analysis of only this pathway for ethanol metabolism. Important regulatory steps considered in the model are shown in Figure 2.

2.2 Effects of Ethanol Metabolism

Irrespective of the mechanism, ethanol is converted to acetaldehyde in liver, which is then oxidized by aldehyde dehydrgenase (ALDH) to acetate. A fraction of acetate is converted to acetyl CoA while more than 60% of acetate diffuses back into the bloodstream [69]. The reactions catalyzed by ADH and ALDH each convert one NAD^+ to one NADH, producing a significant imbalance in redox ratios, which disturbs a large number of metabolic processes. The excess NADH affects the lactate to pyruvate ratios, driving the equilibrium reaction towards lactate. Thus more pyruvate goes to lactate,

which results in low gluconeogenic fluxes [35, 39, 40, 51, 53]. These pathways are shown in Figure 2.

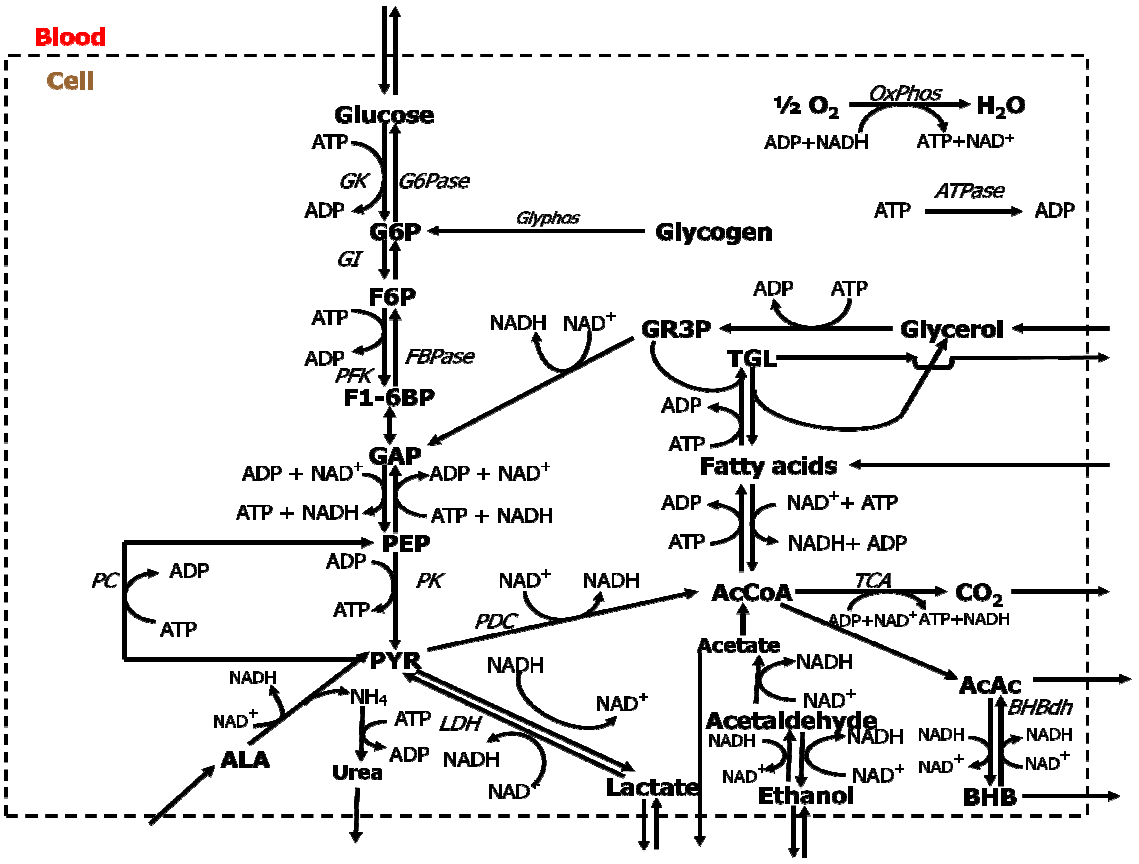

Figure 2. Metabolic pathways showing important regulatory steps in the comprehensive model of ethanol metabolism.

Other major effects include triglyceride accumulation, which subsequently results in alcoholic liver cirrhosis. Excess NADH stimulates the synthesis of glycerol from glycolytic intermediates. Acetyl CoA accumulation increases the rate of ketone bodies production. High NADH concentration also inhibits enzymes of the TCA cycle, further deteriorating metabolic functions. Acetaldehyde not converted to acetic acid can bind to cysteine, a constituent of the anti-oxidant peptide glutathione (GSH) which further

compromises liver mitochondrial functions with oxidative damage. Acetaldehyde released into the bloodstream can drift to other organs like brain, where it can damage proteins and DNA synthesis as well as lipid peroxidation in cell membranes [56, 66].

The aim of this thesis is to show the quantitatively effects of ethanol metabolism on lactate to pyruvate ratio and gluconeogenic fluxe.

2.3 Previous Models of Ethanol Metabolism

A number of pharmacokinetic models of ethanol metabolism are described to contribute to the understanding of ethanol clearance in human beings. Most of these fail to account for acetaldehyde, which is an important toxic metabolite of ethanol metabolism [41, 43, 44]. Fogler [45] presented a well-recognized, physiologically-based pharmacokinetic model for ethanol and acetaldehyde metabolism. The model is highly impressive in terms of their approach for modeling and compartmentation in which liver is considered as tubular reactor while the stomach, gastrointestinal tract, central fluid, and muscle are considered as well-stirred reactors. But their rate laws for alcohol dehydrogenase (ADH) and acetaldehyde dehydrogenase (ALDH) are missing important characteristics such as ethanol substrate inhibition, NADH product inhibition for ADH and NAD^+ control of ALDH. In all previous attempts of modeling ethanol metabolism, no attempts were made to quantify the effects of ethanol on glucose metabolism and lactate uptake.

In contrast to our lumped modeling approach, several authors have presented other methodologies such as steady state flux balance analysis (FBA) in combination with either Fischer discriminant analysis or optimization of a presumed objective

function. All these models contain reactions describing hepatic metabolism which provide insight into the distribution of fluxes over a range of steady states. All these approaches use experimental measurements of fluxes as inputs. Absence of reaction kinetics questions the reliability of these methodologies. A space - distributed modeling approach is actually one of the best possible representation of liver metabolism, since it accounts for the heterogeneity in enzyme distribution, differential flow rates, and concentrations of metabolites across the liver. However, limited availability of experimental data makes it nearly impossible to develop and validate a distributed model.

2.4 Role of PFK – FBPase Substrate Cycle

The reactions catalyzed by phosphofructokinase-1 (PFK) and fructose 1,6 bisphosphatase (FBPase) are the most significant step for controlling the relative rates of glycolysis and gluconeogenesis. Tight control is accomplished through allosteric effects (effect on the enzyme by species other than the substrate or product of the reaction at a site other than the protein's active site) of fructose-2,6 bisphosphate (F2,6BP) and AMP on both enzymes, substrate inhibition of PFK by ATP, and glucagon-controlled cAMP-dependent phosphorylation of FBPase. These complex control mechanisms prevent the simultaneous operation of both enzymes, which otherwise would lead to substrate cycling and concomitant ATP hydrolysis.

Numerous kinetic studies of these two enzymes have been reported [3, 4, 11, 16, 18]. Most of these studies put emphasis on collecting *in vitro* kinetic data that reveal the complex behavior of the enzymes and describe the binding pattern of the allosteric activators and inhibitors. While each of these studies usually reported values for specific kinetic parameters based on the experimental conditions investigated, comprehensive

quantitative models that consider the more recent knowledge of these enzymes, which are necessary for a complete understanding of the coordinated regulation of the cycle, are lacking. Furthermore, a realistic model should correctly predict the relative fluxes for a wide range of substrate and allosteric effector concentrations. Moreover, these kinetic models play key roles in comprehensive *in silico* models of liver metabolism under development [33].

CHAPTER III

KINETIC MODELS OF PHOSPHOFRUCTOKINASE AND FRUCTOSE-1,6-BISPHOSPHATASE

3.1 Model Development

The most complete quantitative model of the regulation of PFK and FBPase , consisting of detailed kinetic descriptions of the two enzymes, was developed by Garfinkel before the discovery of F2,6BP and its important regulatory role in regulation [18]. This work also did not include the effect of phosphorylation, which has been found to be important in the regulation of FBPase.

The regulatory mechanism of PFK and early mathematical descriptions have been reported by several groups. Brand and Soling [6] examined the kinetics of this enzyme under conditions of very low ATP concentrations at pH 8 (where it did not exhibit any allosterism) and calculated true Michaelis and inhibition constants based on an approximate ordered bi bi reaction mechanism at low product concentration. Reinhart and Lardy [30] studied kinetic activity of the enzyme under near-physiological conditions. Since these studies were done before the discovery of F2,6BP, their models

lack this potent influence. The effect of F2,6BP was considered, along with calculation of the Km for fructose-6-phosphate (F6P) and substrate inhibition by ATP, in a later model of PFK by Reinhart [16]. However, this model did not include AMP activation and its synergism with F2,6BP, resulting in an unrealistically large estimation of the half velocity constant for F6P.

The allosteric regulation of FBPase has been modeled by means of a three state binding model based upon the simple Monod equation [3]. However, no attempt was made to compute the values for the parameters of the model. Francois et al. [4] also proposed a model to describe the binding pattern of rat liver FBPase, but again the parameter values were not computed.

The objective of the work presented here is to develop model equations that exhibit the most important regulatory characteristics known of the two enzymes, PFK and FBPase. These equations build upon previous models, especially that of Garfinkel, and incorporate up-to-date information about the enzymes. Model parameters are calculated using data from *in vitro* kinetic studies. With these comprehensive kinetic models, simulations are performed to investigate and quantify the effects of various regulators on cycling and net throughput through the F6P – F16BP system, and thus to better understand the control mechanism for glycolysis and gluconeogenesis. Furthermore, these kinetic expressions play key roles in our model of gluconeogenesis and lipid metabolism in the liver.

3.1.1 Phosphofructokinase

PFK is subjected to strong metabolic control by a number of positive and negative effectors that include fructose 1,6 bis-phosphate (F1,6BP), F2,6BP, AMP, MgATP, H^+

and citrate. With detailed literature review we identified important kinetic characteristics of PFK: 1) substrate inhibition of PFK by the high concentration of ATP; 2) activation by F2,6BP; 3) activation by AMP; 4) interrelation between activation of PFK by F2,6BP and AMP; 5) the fact that F2,6BP and AMP relives the inhibition of the enzyme by high concentration of ATP [1, 2, 4, 11, 12]. These regulations are shown in Figure 3.

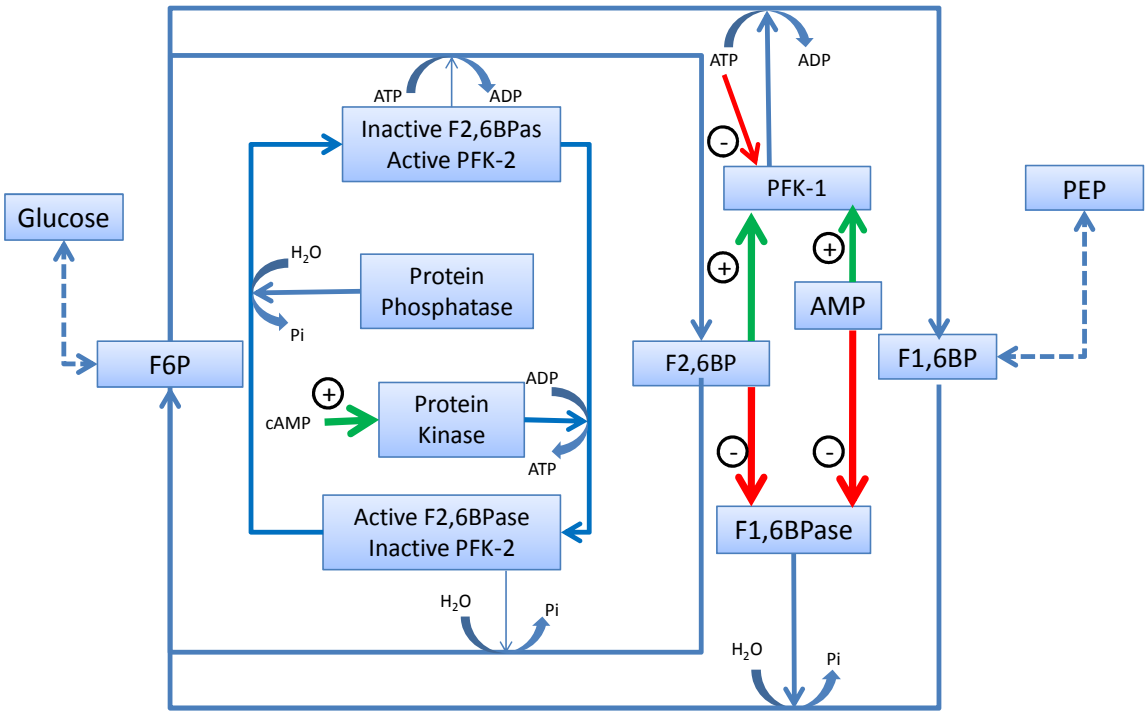

Figure 3 Regulation of PFK – FBPase substrate cycle with the bifunctional enzyme

Kinetic data suggested an ordered bi- bi reaction mechanism, with F6P as the first substrate to attach, followed by ATP (which is an inhibitor as well), and ADP as the first product to be released, followed by F1,6BP [6]. Since the products of the PFK reaction, F1,6BP and ADP, play only a minor role in deciding the rate of reaction [1], we started

with the approximat ordered bi-bi reaction mechanism at low product concentrations assuming rapid equilibrium [15]:

$$\frac{v}{V_{max}} = \frac{[F6P][ATP]}{K_{iF6P}K_{mATP} + K_{mATP}[F6P] + K_{mF6P}[ATP] + [ATP][F6P]} \tag{3.1}$$

Simplifying this expression further we proposed:

$$\frac{V}{V_{\max}} = \frac{[ATP]\cdot[F6P]}{K + [ATP]\cdot[F6P]} \tag{3.2}$$

PFK has low affinity and high degree of cooperativity for its substrate F6P in the absence of any effecter [6], based on this fact we raised F6P to the 2nd power as shown in equation (3.3).

$$\frac{V}{V_{\max}} = \frac{[ATP]\cdot[F6P]^2}{K + [ATP]\cdot[F6P]^2} \tag{3.3}$$

To enforce further regulation of substrate inhibition by ATP and activation by F2,6BP and AMP, we modified the kinetic constant K in equation (3.3). The substrate inhibition can be represented by a classical expression with assumption of rapid equilibrium as [15]:

$$v = \frac{V_m[S]}{K'_m + [S] + \frac{[S]^2}{K_{S1}}} \tag{3.4}$$

Using this equation for ATP substrate inhibition we modified the K of equation (3.3). The complete substrate inhibition term of ATP, in equation (3.5) is raised to the 2nd power to increase sensitivity of relative velocity of reaction to the high concentration of ATP, resulting in:

$$K = K_{F6P}^{app}\left([ATP] + K_{ATP} + \frac{[ATP]^2}{K_{iATP}} \right)^2 \tag{3.5}$$

We selected equation used by Reinhart et al [16] to represent activation of the enzyme PFK by F2,6BP and AMP concentrations. These equations are shown as terms T_1 and T_2 in equation (3.6) and (3.7). These terms, T_1 and T_2 are raised to the power n1 and n2 respectively, to alter the sensitivity of activation by F2,6BP and AMP. Thus at high F2,6BP concentration $T_1 \rightarrow \alpha/Q_1$ and at low F2,6BP concentration $T_1 \rightarrow \alpha$. Similarly at low ATP concentration $T_2 \rightarrow \sigma$ and at high AMP concentration $T_2 \rightarrow \sigma/Q_2$. In these expressions, α and σ are the extra binding constants and Q_1 and Q_2 are the coupling parameters which describe the nature and magnitude of the effects of each allosteric ligand on the binding of substrate F6P to enzyme. If $Q < 1$ the allosteric ligand is an inhibitor, if $Q > 1$ the allosteric ligand is an activator, and if $Q = 1$ then the allosteric ligand has no effect on substrate binding [16]. The dissociation constant for F2,6BP and AMP in the absence of F6P is represented by $K_{iF2,6BP}$ and K_{iAMP} respectively[16].

$$T_1 = \alpha\left(\frac{K_{iF2,6BP} + [F2,6BP]}{K_{iF2,6BP} + Q_1[F2,6BP]} \right)^{n1} \tag{3.6}$$

$$T_2 = \sigma\left(\frac{K_{iAMP} + [AMP]}{K_{iAMP} + Q_2[AMP]} \right)^{n2} \tag{3.7}$$

F2,6BP is the most potent activator with a complex regulatory pattern. F2,6BP (more prominently than AMP) relieves the substrate inhibition of ATP; this can be described by the product of terms T_1 and $[ATP]^2/K_{iATP}$. F2,6BP increases the affinity of F6P for the enzyme, but has no effect on maximal activity of PFK. F2,6BP and AMP

both individually and together overcome the inhibition by high concentration of ATP, which can be achieved with the separate term *(1 + T_1 + T_2)*. F2,6BP acts synergistically with AMP to relieve ATP inhibition thus potentiating activation by AMP [9]. Both AMP and F2,6BP act synergistically to decrease the half velocity constant for substrate F6P. To account for all these effects we proposed an equation for half velocity constant K as:

$$K = K_{F6P}^{app}\left([ATP] + K_{ATP} + T_1 \frac{[ATP]^2}{K_{iATP}} \right)^2 \left(1 + T_2 + T_1\right) \tag{3.8}$$

The effect of phosphorylation on the kinetic properties of PFK is still an open question [29], and has not been considered here. The influences of citrate, F1,6BP, and ADP are also neglected since these interactions are less significant as compared to those of ATP, AMP, and F2,6BP [1, 2, 16]. The complete model is shown in expression (3.9)

$$\frac{V}{V_{\max}} = \frac{[ATP] \cdot [F6P]^2}{K + [ATP] \cdot [F6P]^2} \tag{3.9}$$

where

$$K = K_{F6P}^{app}\left([ATP] + K_{ATP} + T_1 \frac{[ATP]^2}{K_{iATP}} \right)^2 \left(1 + T_2 + T_1\right) \tag{3.9.a}$$

$$T_1 = \alpha\left(\frac{K_{iF2,6BP} + [F2,6BP]}{K_{iF2,6BP} + Q_1[F2,6BP]} \right)^{n1} \tag{3.9.b}$$

$$T_2 = \sigma\left(\frac{K_{iAMP} + [AMP]}{K_{iAMP} + Q_2[AMP]} \right)^{n2} \tag{3.9.c}$$

3.1.2 Fructose-1,6-Bisphosphatase

F2,6BP, a known powerful activator of PFK, is a strong inhibitor of FBPase. The main characteristics of the enzyme are: the inhibition is much stronger at low substrate concentration; inhibition of the enzyme by AMP is enhanced by F2,6BP (indicating allosteric type inhibition), and F2,6BP changes the substrate saturation curve from almost hyperbolic to sigmoidal [2,5,9,29]. Meek and Nimmo [3] have shown that F2,6BP can bind at two distinct sites, catalytic and regulatory, and at high concentration of F2,6BP in combination with high concentration of AMP, the kinetic response of the enzyme to F1,6BP reverts to hyperbolic. Further they mentioned that inhibition of FBPase by AMP is uncompetitive with respect to F1,6BP in the absence of F2,6BP, but non-competitive in its presence. However, others [5,7] have shown that F2,6BP binds only to the catalytic site with higher affinity than F1,6BP, which brings about a conformational change in the enzyme that facilitates AMP binding. FBPase is also regulated by ADP and ATP, but much higher concentrations of these nucleotides is needed than of AMP for a similar effect [7].

The influence of phosphorylation on the activity of F1,6BPase has been a subject of some dispute. Some groups have observed essentially no change in the activity of the enzyme with phosphorylation [8,9], while others have detected increase in Vmax, and decrease in apparent Km for substrate with phosphorylation [7,20]. FBPase is known to be phosphorylated *in vitro* by cAMP-dependent protein kinase. It has been shown that the unphosphorylated FBPase is more susceptible to inhibition by AMP and F2,6BP than is the phosphorylated F1,6BPase [7,20]. In our model we accounted for the effect of phosphorylation on the enzyme by considering the variations in the cAMP

concentrations. The rat liver *in vivo* cAMP level is expected to vary from 0.008 mM in fasted state to 0.0012 mM in the fed state [34].

Classical Monod, Wyman, and Changeux transition model (MWC Model) is considered as the basis for developing this model for FBPase because of its ability to deal with allosteric interactions and phosphosrylation [15]:

$$\frac{v}{V_{max}} = \frac{\alpha(1+\alpha)^{n-1}}{L' + (1+\alpha)^n} \tag{3.10}$$

where $\alpha = [s]/K_s$, the substrate concentration to kinetic constant ratio,

The number of enzyme subunits, containing one catalytic site each, is approximately represented by n. L is the allosteric constant – the equilibrium constant of the free form of the low substrate affinity conformation of the enzyme (T-state) and the high substrate affinity conformation (R-state).

The MWC model shown in equation (3.10) is then modified by introducing additional terms for cAMP, AMP and F2,6BP:

$$\alpha = \frac{[\text{F1,6BP}]}{\text{K}_{sF1,6BP}}, \beta = \frac{[\text{F2,6BP}]}{\text{K}_{iF2,6BP}}, \gamma = \frac{[c\text{AMP}]}{\text{K}_{icAMP}}, \sigma = \frac{[\text{AMP}]}{\text{K}_{iAMP}}$$

In the absence of the inhibitors F2,6BP and AMP, phosphorylattion does not affect Vmax of FBPase but in the presence of either of the inhibitors Vmax of FBPase is appreciably different [7,20]. To account for this effect, the term is proposed as a multiplier of Vmax in equation (3.10)

$$T_3 = \frac{(1+\beta\gamma+\sigma\gamma)^n}{(1+\beta)^n(1+\sigma)^n} \tag{3.11}$$

Both inhibitors F2,6BP and AMP act synergistically, with F2,6BP enhancing the effect of AMP inhibition, This effect is represented by the product of the terms $(1+\beta)$ and (1+σ) for F2,6BP and AMP in the denominator of $(1+\beta\gamma+\sigma\gamma)$ term.

F2,6BP is a competitive inhibitor and hence it must be also combined with the allosteric constant *L* in the denominator of the MWC expression (3.10). Phosphorylation of the enzyme by cAMP-dependent protein kinase increases the activity of the enzyme by decreasing its apparent Km for F1,6BP. This can be achieved by dividing the allosteric constant L by $(1+c\gamma)$, where the quantity *c* is the non-exclusive binding coefficient used for controlling the extent of phosphorylation by cAMP. Thus the allosteric constant L of the MWC expression is modified to:

$$L' = L\frac{(1+\beta)^n}{(1+c\gamma)^n} \tag{3.12}$$

The final equation resulting from all these hypothetical arrangements, based on understanding of the FBPase kinetic characteristics is shown in equation (3.13):

$$\frac{V}{V_{max}} = \frac{\dfrac{\alpha(1+\alpha)^{n-1}}{(1+\beta)^n(1+\sigma)^n}(1+\beta\gamma+\sigma\gamma)^n}{L\dfrac{(1+\beta)^n}{(1+c\gamma)^n}+(1+\alpha)^n} \tag{3.13}$$

Where,

$$\alpha = \frac{[\text{F1,6BP}]}{K_{sF\,1,6\,BP}}, \beta = \frac{[\text{F2,6BP}]}{K_{iF\,2,6\,BP}}, \gamma = \frac{[c\text{AMP}]}{K_{icAMP}}, \sigma = \frac{[\text{AMP}]}{K_{iAMP}}$$

L - Allosteric constant

c - Non-exclusive binding coefficient

The sensitivity of the activity v_i of each enzyme i, relative to each parameter $K_{i,j}$ in the kinetic model was defined as $S_{vi,Ki,j}$, given by:

$$S_{vi,Ki,j} = \frac{\partial v_i / v_i}{\partial K_{i,j} / K_{i,j}} \tag{3.14}$$

The sensitivities were calculated using the central difference method, at concentrations representative of the fed and fasted states.

3.2 Results

While numerous groups have obtained kinetic data on PFK from liver, the data reported by Van Schaftingen et al. [1] is among the most comprehensive and includes effects of F2,6BP and AMP. Moreover, their study was performed at near physiological concentrations of metabolites, which is important if the model expression is to be applicable *in vivo*. The kinetic parameters for PFK were obtained by fitting Eqn. 3.9 to their data using the generalized reduced gradient method in microsoft excel. Parameter estimation for Eqn. 3.13 (FBPase) was performed using *in vitro* kinetic data obtained by Ekdahl et al. [20], with an emphasis on data obtained for physiological ranges of metabolites. Estimated parameters and confidence intervals are shown in Tables I and II.

Table I Parameter values with confidence intervals in the PFK model (Eqn. 3.9).

α	2	+/- 1.88E+01
σ	3.5	+/- 8.63E+01
K_{ATP} *(mM)*	0.05	+/- 1.77E+00
K^{app}_{F6P} *(mM)*	0.0007	+/- 1.84E-03
K_{iATP} *(mM)*	1	+/- 2.05E+01
n1	3	+/- 2.77E+01
n2	3	+/- 5.64E+01
$K_{iF2,6BP}$ *(mM)*	0.03	+/- 7.74E+00
Q1	100	+/- 2.65E+04
K_{iAMP} *(mM)*	2	+/- 3.77E+02
Q2	50	+/- 1.04E+04

Table II Parameter values with confidence intervals in the FBPase model (Eqn. 3.13).

$K_{sF1,6BP}$ *uM*	1	+/- 1.80e+000
K_{iAMP} *uM*	182.20	+/- 1.35e+001
$K_{iF2,6BP}$ *uM*	30	+/- 9.23e+000
K_{icAMP} *uM*	20	+/- 6.60e+001
L	2.76E+06	+/- 1.00e+007
n	5.52	+/- 1.69e+000
c	0.56	+/- Inf

The relative activities of PFK predicted by Eqn. (3.9) are shown in Figure 4 along with the data obtained from the *in vitro* experiments. In general, the model captures the important trends of the data as well as other known regulatory effects, in terms of activation by F2,6BP (Figure 4A-D), substrate inhibition by ATP (Figure 4B), activation by AMP (Figure 4D), and hyperbolic dependence on the two substrates at high F2,6BP concentrations (Figure 4A,C). At low concentrations of F2,6BP the model shows proper cooperative behavior of the enzyme for substrate F6P (Figure 4A) and for F2,6BP as well (Figure 4D).

Figure 4B shows the expected reduction of ATP-substrate inhibition by F2,6BP. The synergism between activation by AMP and F2,6BP are demonstrated in Figure 4C. While a very good correspondence between model and data are shown for most of the concentration ranges, the model greatly underestimates activity at AMP greater than 0.4 mM and F2,6BP at 0.25 μM or less. However, this region is at AMP concentrations greater than that occurring *in vivo* (0.1 – 0.3 mM) [5,12,13,17,18], and at F2,6BP concentrations in the low range of *in vivo* concentration (0.1 to 10 μM) [16,17], so analyses using this model at *in vivo* conditions can be presumed to be valid. The

interaction of F2,6BP with AMP, at more physiological concentrations, is demonstrated in Figure 4D, with good correspondence between data and model.

Simulations of FBPase activity using Eqn. (3.13) are shown in Figure 5 in comparison to *in vitro* data. The inhibition by F2,6BP and the positive effect of phosphorylation are captured almost perfectly, as shown in Figure 5A, which also demonstrates that phosphorylation is ineffective at saturating concentrations of substrate. The substrate-dependency is predicted well (Figure 5A,B,C), except at the unphosphorylated state at high concentrations of F2,6BP, where no FBPase activity was measured (Figure 5C). Since FBPase is homotetramer [3,7,8], the expected value of n is 4, although the value that resulted in the best fit was actually 5.5, indicating that the MWC model is not a rigorously correct description of the mechanism.

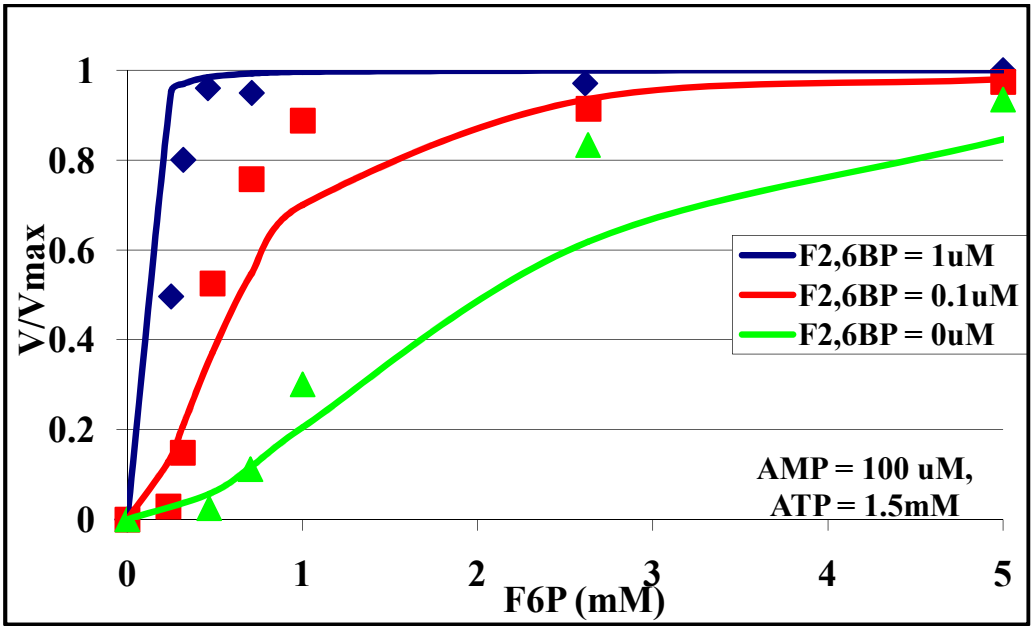

Figure 4 (A)

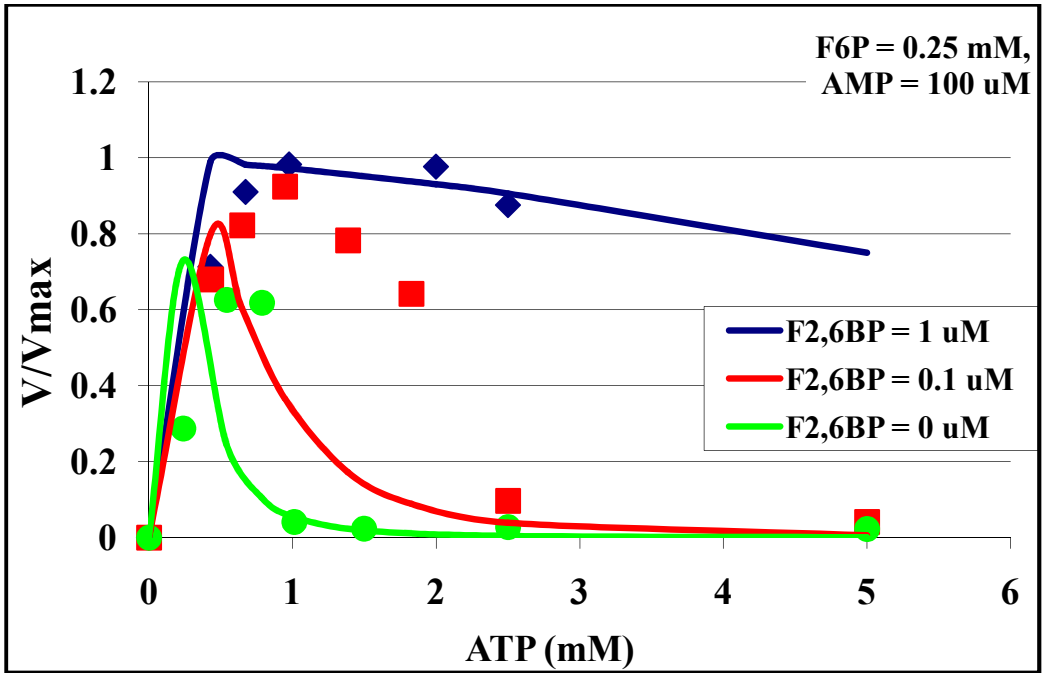

Figure 4 (B)

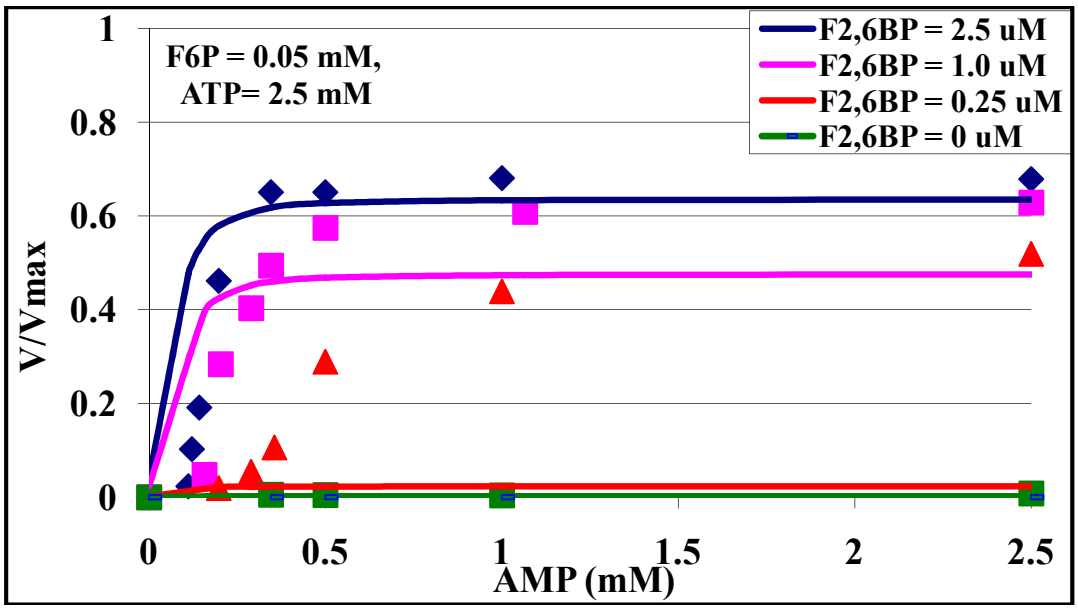

Figure 4 (C)

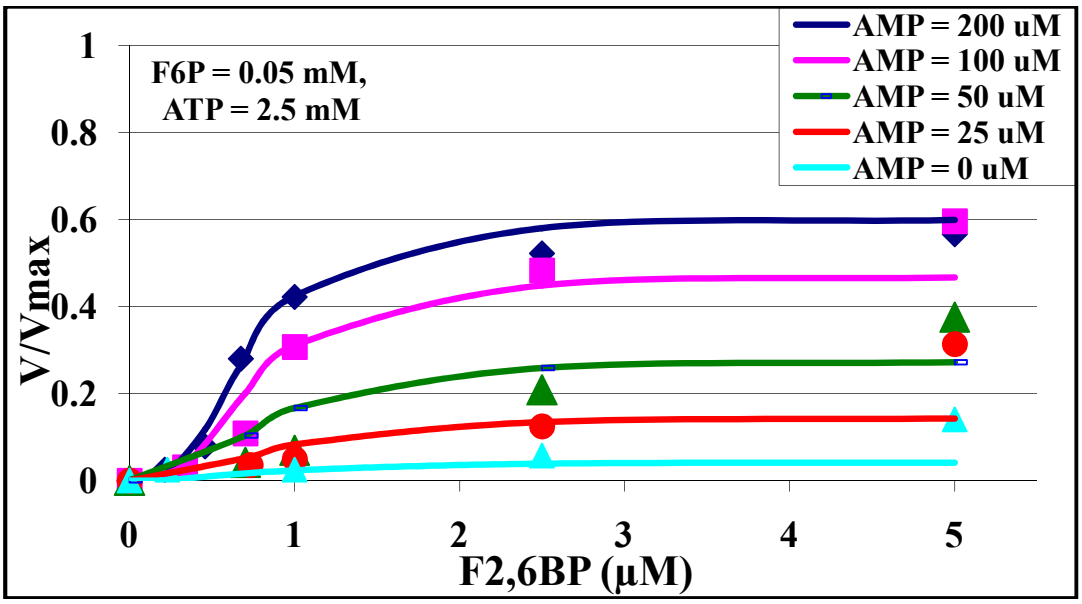

Figure 4 (D)

Figure 4 Simulation results for phosphofructokinase kinetic model (Eqn.3.9).The in vitro data used for developing the model with the corresponding model calculated outputs are shown in the figure. Effect of F2,6BP on the affinity of PFK for substrate F6P (A) and on inhibition of PFK by substrate ATP (B). Figures. (C) and (D) show effects of F2,6BP and AMP on relative velocity of PFK. Simulation results are continuous lines, corresponding experimental data are represented as points with the same color. Other metabolite concentrations are as shown on the Figure. The data is from Van Schaftingen et al. [1].

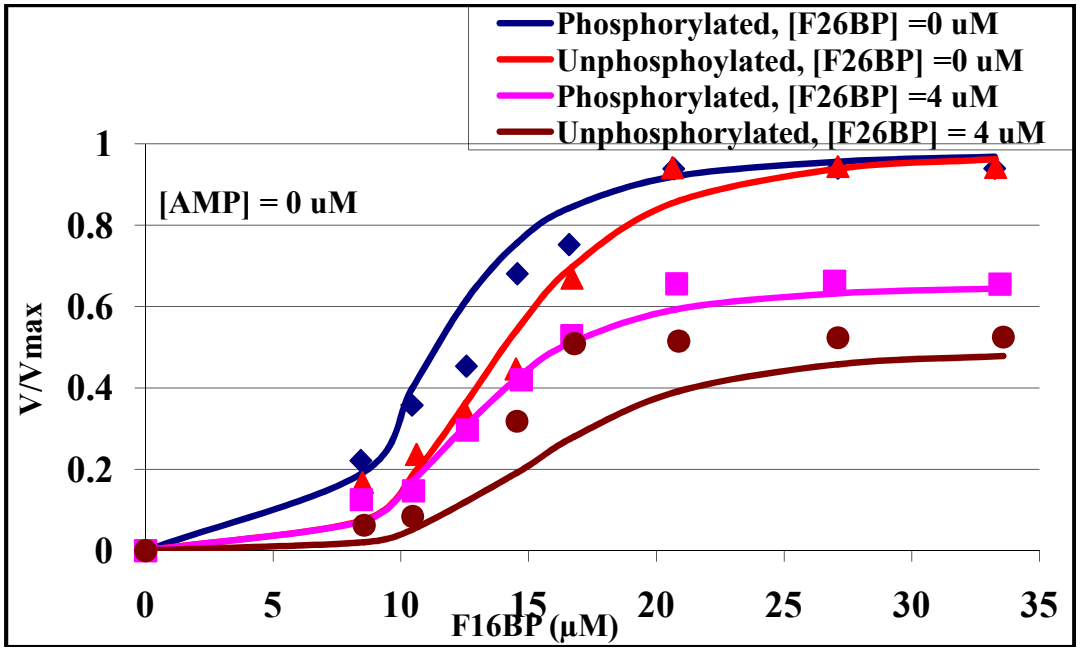

Figure 5. (A)

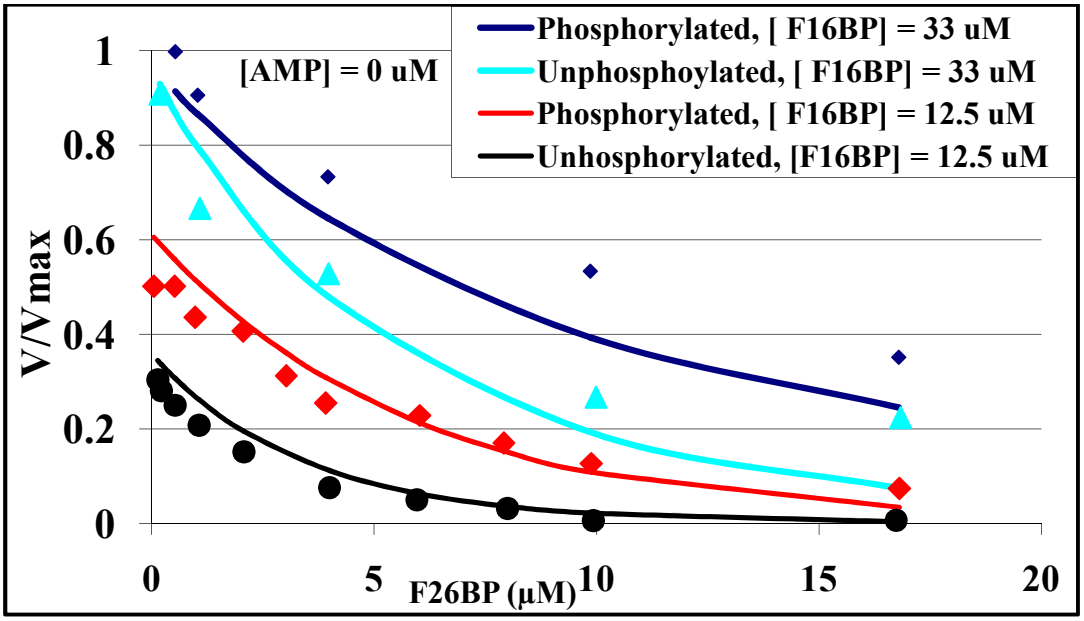

Figure 5. (B)

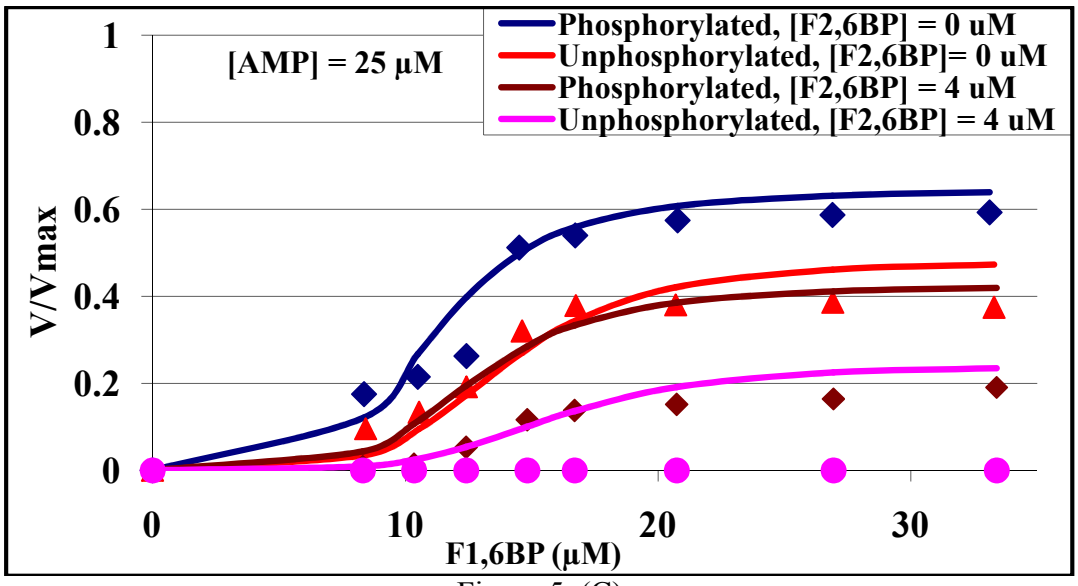

Figure 5. (C)

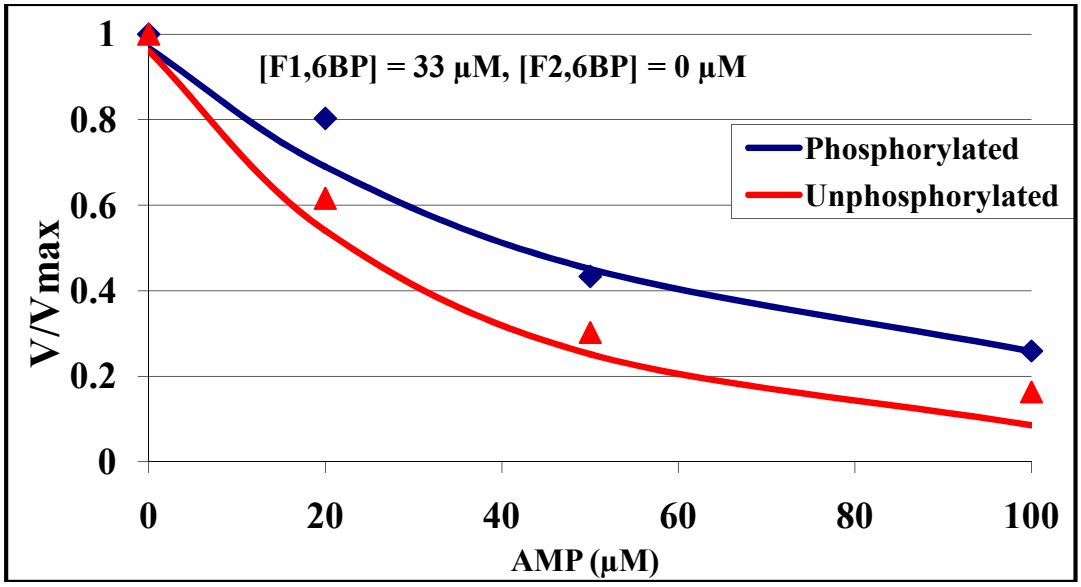

Figure 5. (D)

Figure 5. Simulation results for F1,6BPase model, Eqn. (3.13). The *in vitro* experimental data (data points) along with the model calculated outputs (continuous lines) for FBPase is shown in fugure. (A) Inhibition of rat liver phosphorylated and unphosphorylated F1,6BPase by F2,6BP at two different concentrations of F1,6BP, 33 and 12.5 µM respectively. (B) and (C): effects of AMP and F2,6BP on the flux of F1,6BPase at different concentrations of substrate F1,6BP. (D) shows activity of phosphorylated and unphosphorylated enzyme at different AMP concentrations. The cAMP concentration used in the model results for phosphorylated enzyme is 0.0075 µmol/gww (16 µM) [34]. Other metabolite concentrations are as shown on the Figure The data are from Ekdahl et al. [20].

Simulations of the fluxes through PFK and FBPase at physiological concentrations of metabolites, in the fed and fasted states, using Eqns (3.9) and (3.13), are shown in Figure 6. Figure 6A shows the fluxes as a function of the ATP/ADP ratio, where the total nucleotide concentration is kept constant. The two rates are relatively independent of the ATP/ADP ratio near the value of 5.9 (measured in the cytosol in the starved state [19]), indicating little control by this quantity at physiological conditions. As expected, the rate of PFK is almost completely inhibited in the fasted state, while the flux in the fed state is activated to 1.11 μmol/gww/min. Conversely, the FBPase is inhibited in the fed state to 0.11 μmol/gww/min and activated in the fasted state to 0.89 μmol/gww/min. The net rate of glycolysis in the fed state is close to that measured *in vivo* 1.0 μmol/gww/min [23-27,31], with about 10 - 15 % of the carbon recycled through the futile cycle. In the fasted state, the net rate of gluconeogenesis is 0.9 μmol/gww/min, which is approximately double that expected for an *in vivo* 24 hour fasted state, [32] with no futile cycling, which is in agreement with previous predictions [28]. These results were calculated with the FBPase Vmax of 16 μmol/gww/min. The measured maximal activity of FBPase from liver tissue actually has a large range (16 ±7 μmol/gww/min) [22], which greatly influences the results obtained.

The regulatory effects of F2,6BP and AMP on the two enzymes are shown in Figure 6C-D. It can be observed in Figure 6C that high concentrations of F2,6BP relieves the substrate inhibition by ATP of PFK at physiological concentrations of all other metabolites. This is a very important property of the enzyme behavior *in vivo*, as mentioned earlier. Note that the greatest amount of futile cycling occurs in the mid-range of F2,6BP concentration, with little futile cycling at the two extreme concentrations of

F2,6BP. Figure 6D shows the effect of AMP on the fluxes. AMP also affects the amount of futile cycling, with most cycling occurring at the lowest AMP concentration.

The sensitivities of PFK flux to the model parameters are shown in Figure 7A. Under fasting conditions, the flux of PFK is very sensitive to changes in α, $K_{iF2,6BP}$, K_{iATP}, $Q1$ and $n1$, while at the fed state the PFK flux is nearly insensitive to the same parameters. Since the flux of PFK at the fasted state is negligible, the large sensitivities at that state have no physical significance. Figure 7B shows that the model for FBPase is highly sensitive to parameters n, K_{iAMP}, and K_{icAMP}. The terms in the MWC model for FBPase (Eqn. 3.13) are raised to the power n, leading to the high sensitivity to this quantity. The phosphorylation state of the enzyme strongly influences its activity, which affects the extent of inhibition by K_{iAMP} and $K_{iF2,6BP}$ and is affected by the cAMP concentration relative to K_{icAMP}.

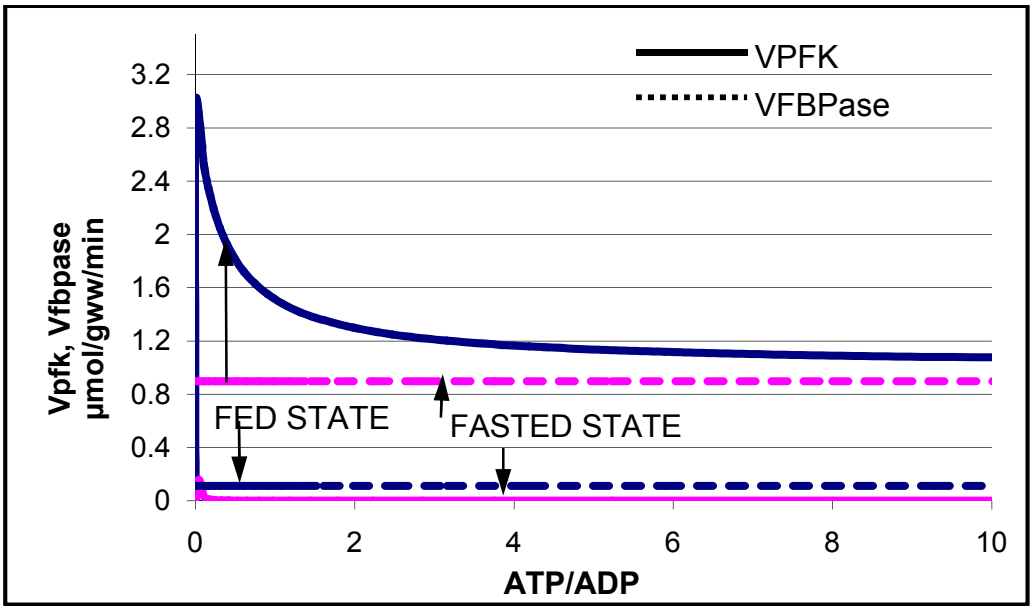

Figure 6 (A)

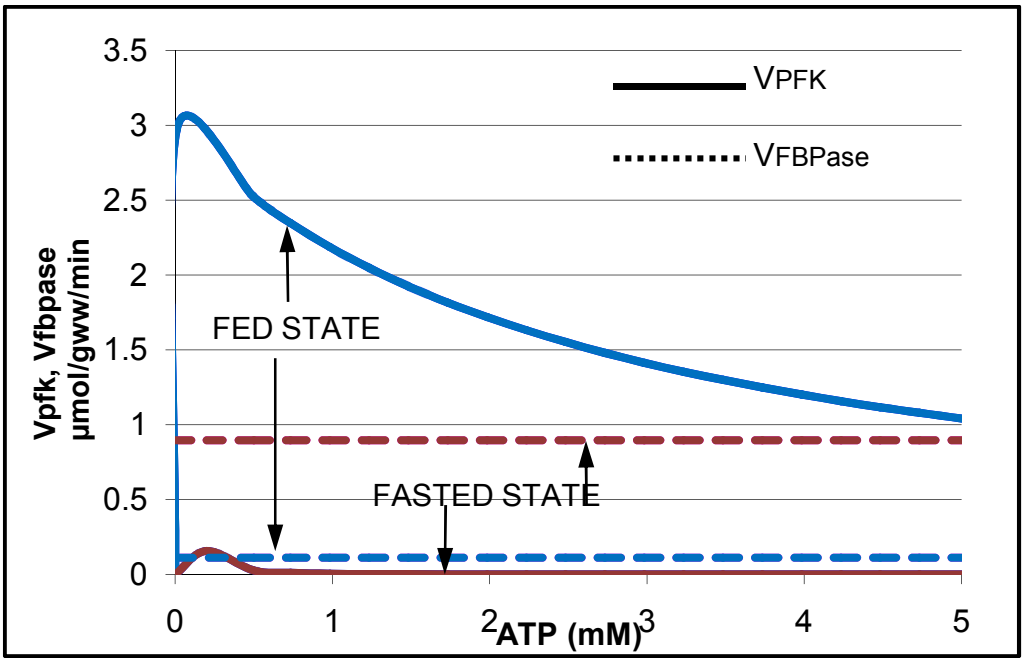

Figure 6 (B)

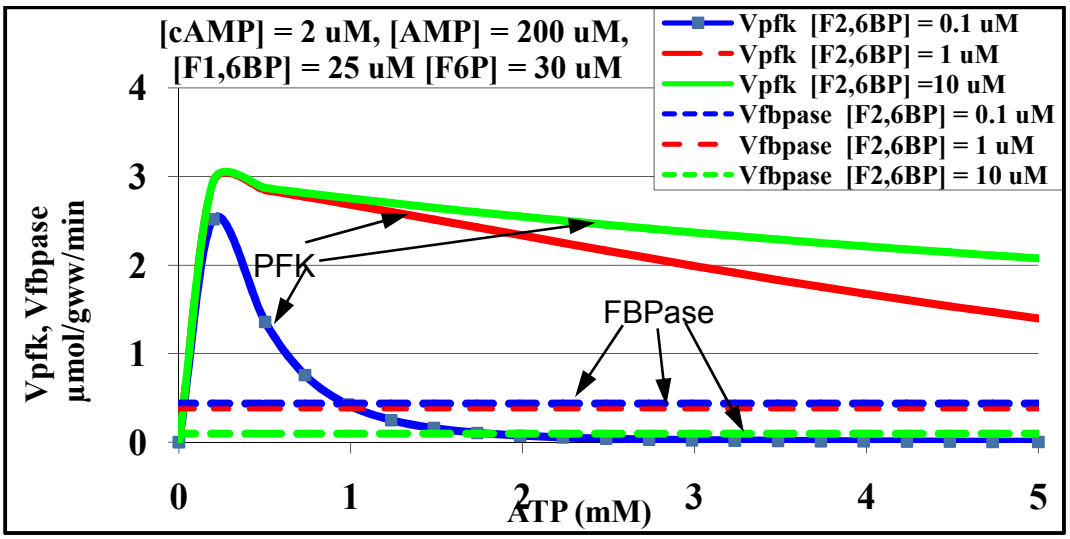

Figure 6 (C)

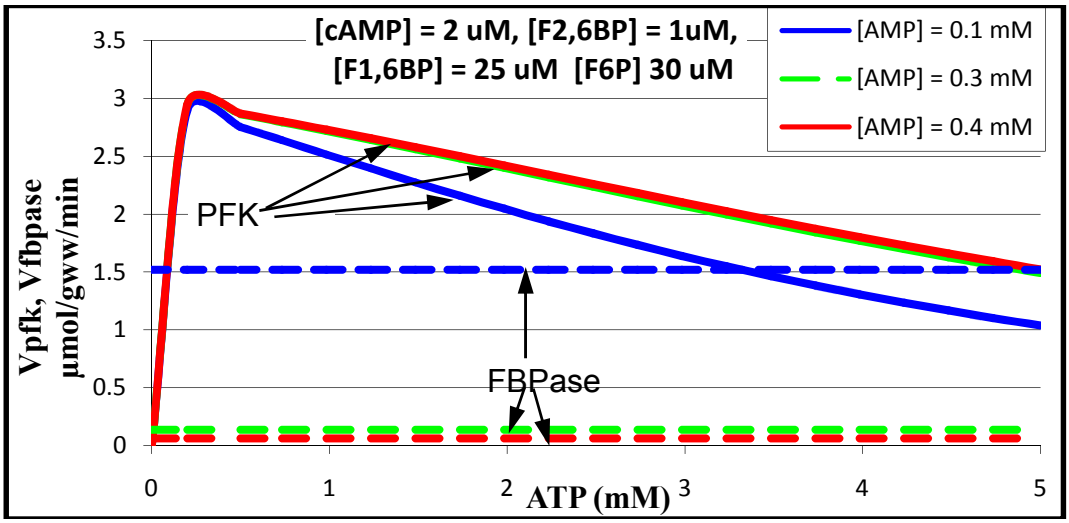

Figure 6 (D)

Figure 6 Simulations results for PFK and FBPase in fed and fasted states, Eqns. (3.9) and (3.13).Species concentrations set equal to values representative of either the *in vivo* fed or the fasted states. Fed state [AMP] = 180 µM [5,12,13,17,18], [F1,6BP] = 46 µM, [14,16,17], [F2,6BP] = 10 µM,[16,17]. [F6P] =0.05 mM [14,18], [cAMP] = 1.2 µM, [34] Fasted state [AMP] = 380 µM,[5,12,13,17,18]. [F1,6BP] = 55 µM, [15,16,17], [F2,6BP] = 0.1 µM,[16,17], [F6P] =0.01 mM,[14,18] [cAMP] = 12 µM.[29]. Vmax for PFK = 3 µmol/gww/min,[21] Vmax for F1,6Bpase = 16 µmol/gww/min.[22] (A) Fluxes as a function of ATP/ADP, keeping the nucleotide sum constant; (B) fluxes as functions of ATP, with all other concentrations constant. (C) Effect of different concentrations of F2,6BP on the fluxes of both the enzymes at different concentrations of ATP. (D) Effect of different *concentrations* of AMP on the fluxes of both the enzymes at different concentrations of ATP. Other metabolite concentrations are as shown on the Figure

Sensitivity Analysis:

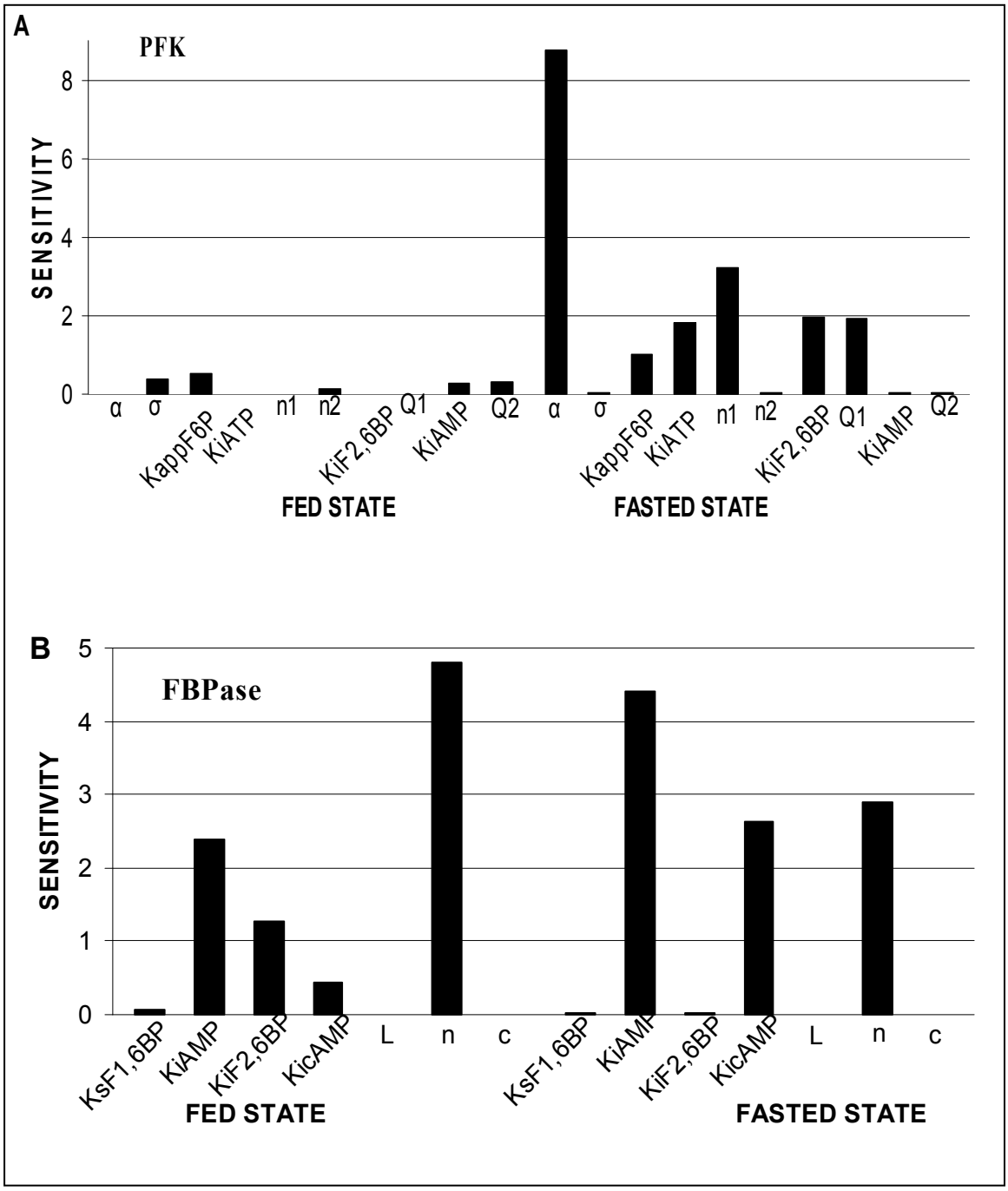

Figure 7 Sensitivity analysis of the kinetic constants to the relative activities of PFK FBPase enzymes in fed and fasted state.

3.3 Discussion

The two model equations presented are based on the most up-to-date findings on the regulatory characteristics of PFK and FBPase, and result in close correspondence with *in vitro* kinetic data, especially for the conditions at the physiological concentrations of metabolites. Although a lot of kinetic data on inhibition and half-velocity constants have been published for these enzymes, the parameters have been reported for specific conditions. Quantitative models for PFK and FBPase that integrate the major kinetic effects, including more recent information such as the effects of F2,6BP on both enzymes and the phosphorylation of FBPase, are not available. After the validation of each kinetic equation, the model was then used to explore the effects of different regulators on the net flux through the system and the expected extent of substrate cycling. The calculated flux of gluconeogenesis is only 10% less than the experimental value in fasted state, this demonstrate the reliability of the model.

PFK – FBPase is probably the most important control site for gluconeogenesis and glycolysis with both short-term and long-term regulation by insulin and glucagon. The increase in glucagon in the fasted state activates adenylyl cyclase, which results in elevation of intracellular cAMP levels, which in turn activates cAMP dependent protein kinase. The cAMP dependent protein kinase then catalyzes phosphorylation of the bifunctional enzyme PFK2/F2,6Bpase and FBpase. The phosphorylation of the bifunctional enzyme decreases F2,6BP levels because of activation of F2,6Bpase and inactivation of PFK2 while the phosphorylation of FBPase later results in its increased activity and hence increased flux of gluconeogenesis. The decrease in F2,6BP directly deactivates PFK and activates FBPase further which again results in increased flux of

gluconeogenesis. These changes also have a potent effect on the other substrate cycle, PEP – pyruvate, since cAMP dependent protein kinase phosphorylates pyruvate kinase, decreasing its activity. Also the decrease in F1,6BP level because of activation of FBpase deactivates PK, both allostericaly (F1,6BP is a strong activator of PK) and by making the enzyme better substrate for phosphorylation by cAMP dependent protein kinase. Thus the F6P – F1,6BP substrate cycle operated by the two enzymes not only affects the rate of gluconeogenesis and glycolysis but also strongly regulates the PEP – pyruvate cycle. We have accounted for the hormonal effects on PFK and FBPase through the terms for F2,6BP and cAMP, and although they are set independently in the equations, they are actually linked *in vivo*, as described above.

The statistical analysis of the two models was done to compute the confidence intervals of the constants. These are reported in Table I and II. It can be observed that the upper and lower limits of the confidence intervals are very large as compared to the parameter values. We used two softwares: excel and matlab to calculate these confidence intervals. Both programs gave the same results. This indicates the existence of singularity which may result from interdependence of the model parameters. This means that the values of the constants in the two kinetic models for PFK and FBPase are not uniquely determined.

The basic aim of our effort to develop the kinetic models for these two enzymes was to account for a number of important *in vivo* regulations. This could have been achieved by using a complex polynomial expression that had constants with small confidence intervals and exactly matched experimental data. But it is important to recognize that the physiological significance of the model structure and parameter values

is of high importance. These expressions are critical part of our comprehensive model of ethanol metabolism. Thus it is important to preserve the significance by keeping these constants near the actual *in vivo* range of the respective substrate concentrations.

The model equations and parameters presented here are useful for understanding metabolic regulation and predicting liver cell behavior when combined with the kinetic descriptions of the other reactions in various pathways in the liver. A model of gluconeogenesis and lipid metabolism in the perfused rat liver, that includes the kinetic equations presented here, has been developed and shown to be predictive of the intermediate concentrations and fluxes in response to perfusion with lactate, pyruvate, and fatty acids. The PFK-FBPase model can be further improved by introducing other known allosteric effectors, such as F1,6BP, ADP, and citrate for PFK, although we expect that this will have little effect on the predictive ability of the *in vivo* model, since these metabolites have a minor role in the regulation of PFK –FBPase. [1, 4, 31].

CHAPTER IV
KINETIC MODELS OF ALCOHOL AND ALDEHYDE DEHYDROGENASE

4.1 Alcohol Dehydrogenase

The physiological role of alcohol dehydrogenase in liver has been puzzling because of the poor stereospecificity of the enzyme for its substrate. Alcohol dehydrogenase catalyzes many reactions involving different types of alcohol, farnesol and certain hydroxy and keto steroids. It has been suggested that oxidation of ethanol is only an occasional activity while the major function of alcohol dehydrogenase is to remove potentially toxic substrates, including ethanol, from circulation and channel them into the pathway of energy supply [35, 36, 37].

As described in the first part of the thesis, in order to predict rates of ethanol elimination at different ethanol concentrations and under different nutritional and endocrinologic conditions we require knowledge of (1) total activity of alcohol dehydrogenase, (2) the contents and specific activity of different forms of the enzyme, if present, (3) kinetic mechanism and constants (i.e., the rate equation) and, (4) in vivo concentration of substrates and products during ethanol metabolism.

Kinetic behavior of alcohol dehydrogenase has been well studied and documented over the last few decades. The reaction catalyzed by alcohol dehydrogenase is essentially a cytosolic reversible reaction, involving substrates ethanol and NAD^+ and products NADH and acetaldehyde [41, 42, 43]:

$$CH_3CH_2OH + NAD^+ \xrightleftharpoons{ADH} CH_3CHO + NADH + H^+$$

There are numerous factors which define the activity of this enzyme in vivo, including age, sex, genetics, and the nutritional state of the body [35]. It has been reported that activity of alcohol dehydrogenase falls to as low as 40% during fasting. Although numerous isoenzymes of alcohol dehydrogenase have been reported (grouped in Class I, II and III), their kinetic behavior is very similar to each other (70-90% homology between the classes) [50]. Therefore, in this attempt isoenzymes of alcohol dehydrogenase are not differentiated, and the activity of alcohol dehydrogenase is its total activity. Alcohol dehydrogenase is found to be inhibited by high concentrations of its substrate ethanol (above 10 mM) and product NADH. Factors influencing the rate of ethanol removal are (1) activity of alcohol dehydrogenase, (2) reoxidation of NADH, and., (3) NAD^+, NADH and ethanol concentrations [42, 43, 57].

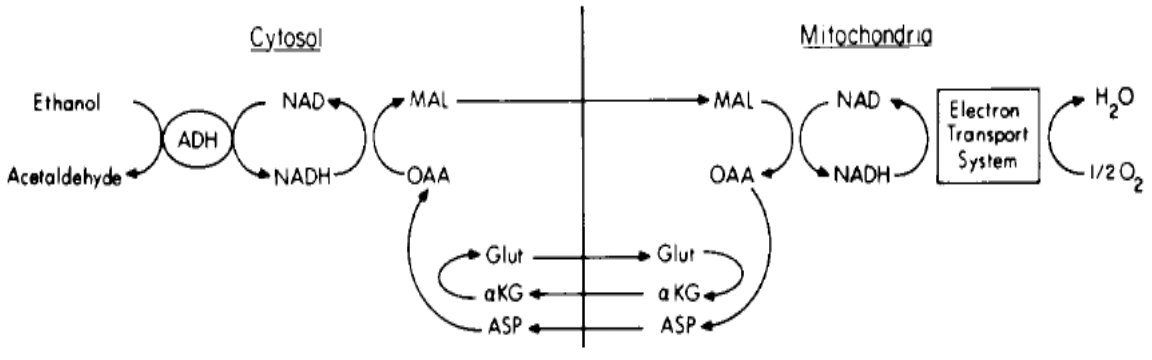

Figure 8. Ethanol metabolism with NADH reoxidation by malate – aspartate shuttle [59].

Activity of alcohol dehydrogenase as motioned before varies significantly with the nutritional state as well as during metabolism. As the alcohol dehydrogenase reaction starts, it drastically alters redox ratios in cytosol, as NAD^+ becomes limiting, high concentrations of NADH produced must be reoxidized to NAD^+ through the malate dehydrogenase shuttle which takes place in mitochondria. Studies of ethanol metabolism strongly suggest that these two factors, namely activity of the enzyme and reoxidation of NADH, are the two most important factors in controlling the rate of ethanol elimination [58, 59]. At high concentrations of ethanol and NADH, a ternary complex of ethanol – ADH–NADH is formed which does not appreciably break down to an ethanol-ADH complex and ultimately does not transform into products [43]. Thus the ADH reaction is inhibited by high concentrations of ethanol and NADH. Other factors such as transport of ethanol from blood to tissue are not considered important because of the complete solubility of ethanol in water [57, 58, 59].

Based on these facts it can be concluded that ethanol elimination is approximately zeroth order with respect to substrate, with substrate inhibition of ethanol and product inhibition by NADH at their high concentrations. This type of behavior is best described by the Theorell – Chance mechanism shown in Figure 9 and equation (4.1) [41, 42].

$$v = \left[\frac{V_f V_r \left([A][B] - \frac{[P][Q]}{K_{eq}} \right)}{K_{ia}K_b + K_b[A] + K_a[B] + [A][B] + K_{ia}K_bK_q[P]/K_pK_{iq} + \frac{K_{ia}K_b[Q]}{K_{iq}} + \frac{K_bK_q[A][P]}{K_{iq}K_p} + \frac{K_{ia}K_b[P][Q]}{K_pK_{iq}} + \frac{K_a[B][Q]}{K_{iq}} + \frac{K_{ia}K_b[B][Q]}{K_iK_{iq}} + \frac{K_a[Q][B]^2}{K_iK_{iq}} + \frac{[A][B]^2}{K_i}} \right] \quad (4.1)$$

where, [A] = NAD^+ [B] = Ethanol [P] = Acetaldehyde [Q] = NADH

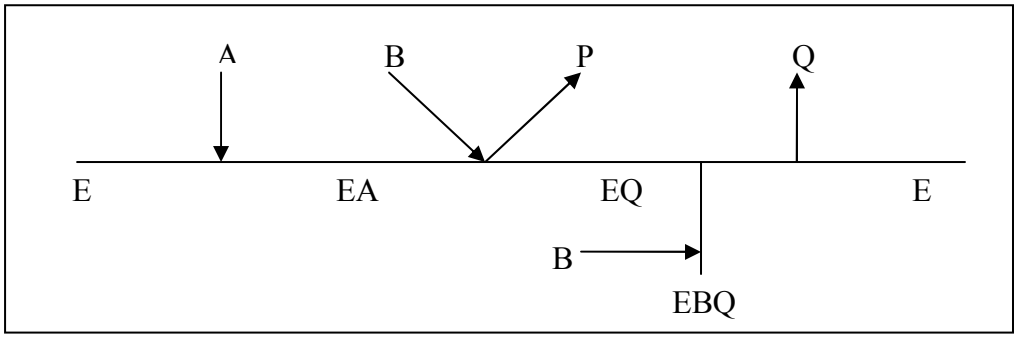

Figure 9 Schematic of the Theorell-Chance mechanism [43].

Table III Kinetic constants of alcohol dehydrogenase model (Eqn. 4.1) [43].

Michaelis Constants *µmol/ghep*	K_b	480E-3
	K_q	4E-3
	K_a	33E-3
	K_p	37E-3
	K_{eq}	1.94E-4
MaximumVelocity *µmol/ghep/min*	V_f	6.71
	V_r	33.62
Inhibition Constants *µmol/ghep*	K_{ib}	810E-3
	K_{iq}	0.9E-3
	K_{ia}	58E-3
	K_{ip}	12E-3
	K_i	1.7E2

Crabb and Bosron [43, 44] extensively studied and justified the use of the Theorell – Chance mechanism for alcohol dehydrogenase. Characteristics such as substrate and product inhibition at their high concentrations making them important regulators, formation of substrate-enzyme- product ternary complex, as well as dead-end pyrazol inhibition are consistent with the Theorell – Chance mechanism. Kinetic constants from the *in vitro* freeze clamped liver study on the fed and fasted animals are reported in Crabbb - Bosron [43, 44]. Predictions of the rate of ethanol elimination using those kinetic constants and a Theorell – Chance mechanism are found to be in agreement with those found *in vivo* and are reported in the same publication.

Some authors have tried to describe the behavior of alcohol dehydrogenase with ordered bi-bi reaction mechanism, which is approximately similar to the Theorell – Chance mechanism, except for the last two terms in the denominator of equation (4.1) [49]. At low concentrations of ethanol both mechanisms yield approximately the same results but at high ethanol concentration (> 10 mM), the Theorell – Chance mechanism shows the important characteristic of substrate inhibition, which is missing in Ordered bi-bi reaction mechanism. For all these reasons we have selected the Theorell – Chance mechanism for the estimation of the rate of the alcohol dehydrogenase reaction in the next chapter of the thesis.

4.2 Aldehyde Dehydrogenase

Unlike alcohol dehydrogenase, which has isoenzymes with identical kinetic constants and overall behavior (in fed and fasted states), isoenzymes of aldehyde dehydrogenase have a very small homology and a strong differential intracellular distribution between the different forms of the enzyme. These isoenzymes of aldehyde

dehydrogenase are grouped into two classes based on their affinity for acetaldehyde as high-K_m aldehyde dehydrogenase ($K_m > 1$ mM) and low-K_m aldehyde dehydrogenase ($K_m \leq 1$ μM). Marjanen [42] reported that 80% of the total activity of aldehyde dehydrogenase is found in the mitochondria while only 20% is found in the cytosol. Moreover, most of the enzyme in the mitochondria is the low-K_m aldehyde dehydrogenase and the cytosolic enzyme is high-K_m aldehyde dehydrogenase.

The reaction catalyzed by aldehyde dehydrogenase is essentially an irreversible reaction involving substrates acetaldehyde and NAD^+ and products NADH and acetate [45, 46, 47]:

$$CH_3CHO + H_2O + NAD^+ \xrightarrow[ALDH]{} CH_3COOH + NADH + H^+$$

The rate of acetaldehyde removal is controlled by the concentration of acetaldehyde, the activity of the enzyme, as well as the NAD^+ concentration available in the respective intracellular compartment. At low acetaldehyde concentration, the NAD^+ control is weaker, since enough concentration of NAD^+ is available for the oxidation of acetaldehyde. However, at high acetaldehyde concentration, NAD^+ plays a significant role in controlling the flux of ALDH reaction. During ethanol metabolism only a small fraction of cytosolic NAD^+ is available for acetaldehyde oxidation, since most of the NAD^+ is utilized for oxidation of ethanol. Svanas and Weiner [46], as well as Williamson [47] reported that acetaldehyde oxidation in rat liver occurs almost entirely in mitochondrial compartment at low to moderate concentrations of acetaldehyde. At high acetaldehyde concentration, however, oxidation may take place in cytoplasm as well. Nevertheless, the amount of acetaldehyde oxidized in mitochondrial compartment is

always much higher than that occurring in cytoplasmic compartment; especially in case of acetaldehyde from ethanol metabolism.

Based on these facts we concluded that a simple Michaelis – Menten equation with some consideration to the NAD^+ control should be enough to describe the kinetic behavior of aldehyde dehydrogenase.

$$v_{ALDH} = \left[\frac{V_{\max}[S] \cdot [NAD^+]}{(K_{m\_S} + [S]) \cdot (K_{m\_NAD} + [NAD^+])} \right] \qquad (4.2)$$

Where S = acetaldehyde

Table IV Kinetic constants of alcohol dehydrogenase model (Eqn. 4.2) [46].

V_{max}	5.3 µmol/ghep/min
K_{m_s}	3.40e-04 µmol/ghep
K_{m_NAD}	0.00928 µmol/ghep

Svanas and Weiner [46] and Fogler [45] used a simple Michaelis –Menten approach (rate of reaction regulated by the enzyme activity only) for estimating rates of acetaldehyde metabolism. Fogler proposed an unsteady state, physiologically based perfusion liver model to predict the rate of acetaldehyde elimination from ethanol in different human body compartments – stomach, GI, liver and so forth. Svanas and Weiner, on the other hand, used experiments with isolated mitochondria of rat hepatocytes and a combined expression of two Michaelis –Menten equations for the low and high K_m acetaldehyde dehydrogenase to estimate the rate of disappearance of acetaldehyde. The rates calculated by Svanas and Weiner at 200 µM acetaldehyde

approximately matched with those found experimentally. Therefore, we used the same kinetic constants estimated by Svanas and Weiner with the assumption that the acetaldehyde is metabolized entirely in the mitochondrial compartment and that the concentration of NAD^+ also regulates the rate of acetaldehyde elimination.

4.3 Transport Mechanism for Ethanol and Acetate

The rate expression used for net transport of ethanol, acetate and other metabolites such as glucose and lactate across the sinusoidal membrane is assumed to be facilitated transport, given by:

$$J_{Etoh\_b\_t,net} = \left[\left(\frac{V_{\max,etoh,b\_t}\left([Etoh]_b - [Etoh]_t\right)}{\left(K_{m\_etoh\_b-t} + [Etoh]_t\right)}\right)\right] \tag{4.3}$$

$$J_{acetate\_b\_t,net} = \left[\left(\frac{V_{\max,acetate,b\_t}\left([acetate]_b - [acetate]_t\right)}{\left(K_{m\_acetate\_b-t} + [acetate]_t\right)}\right)\right] \tag{4.4}$$

The transport constants for expressions (4.3) and (4.4) are show in Table V. Vmax and Km for the transport of both ethanol and acetate are obtained from the literature by referring to the observed rate of ethanol and acetate elimination from blood *in vivo* [69].

Table V Kinetic constants for transport expression for ethanol and acetate.

$V_{max,etoh,b\_t}$	4.3 µmol/ghep /min	From *in vivo* study [69]
$K_{m\_etoh\_b-t}$	0.1 µmol/ghep	Assumed based on expected ethanol concentration *in vivo*
$V_{max,acetate,b\_t}$	4.04 µmol/ghep/min	From *in vivo* study [69]
$K_{m\_acetate\_b-t}$	0.1 µmol/ghep	Assumed based on expected acetate concentration *in vivo*

CHAPTER V

MATHEMATICAL MODEL OF ETHANOL METABOLISM IN LIVER

5.1 Model Development

The purpose of modeling individual kinetic reactions accurately in the previous two sections (for phosphofructokinase, fructose 1,6-bisphosphatase and alcohol and aldehyde dehydrogenase) was to obtain a reasonable flexibility and predictive power for the estimation of concentrations and fluxes through each important regulatory step. This is very crucial especially since significant recycling and complex regulation is involved in these steps. Similar type of models were developed for other important reaction steps like pyruvate kinase, pyruvate carboxylase and pyruvate dehydrogenase complex in our group. Some of the simple, irreversible reactions are expressed with Michaelis – Menten kinetics and introducing the ratios like ADP/ATP and NADH/NAD as relevant. With all this detailed kinetic modeling and in-depth research on the complex regulation of metabolism, we developed the basic building blocks for the lumped model of hepatic metabolism.

The initial challenge was to confirm the effect of lactate and pyruvate perfusion on the gluconeogenic fluxes and metabolite concentrations by comparing the calculated

results with the experimental data available from the literature. This part of the work has been completed by coworkers (published in Chalhoub et al. 2007) [38]. The metabolic pathways considered were glycolysis, gluconeogenesis, citric acid cycle, fatty acid oxidation, fatty acid synthesis, ketogenesis, oxidative phosphorylation, and glycogen degradation, with each pathway represented by a few key reactions, as shown in Figure 2. Ethanol causes enormous turbulence in normal metabolic operations of hepatocytes. It significantly affects almost all these pathways. Thus analyzing the response of the model by adding the ethanol metabolism part can be used to validate the entire model, instead of using different substrates which can stimulate only one pathway.

For the comprehensive lumped model of the perfused rat liver, tissue and blood compartments are considered as two well mixed domains with mass balances for each metabolite as show in equations (5.1), (5.2), (5.3). The mass balance in the tissue domain is given by:

$$\frac{dC_{i,tissue}}{dt} = J_{i,b-t}(C_{i,blood}, C_{i,tissue})\frac{V_{tissue}}{V_{\sin usoid}} + \sum_{j} R_{i,j} \tag{5.1}$$

The mass balance in the blood domain is given by:

$$\frac{dC_{i,blood}}{dt} = (C_{i,perfusate} - C_{i,blood})\frac{F_{perfusate}}{V_{\sin usoid}} - J_{i,b-t}(C_{i,blood}, C_{i,tissue}) \tag{5.2}$$

The mass balance in the perfusate is given by:

$$\frac{dC_{i,perfusate}}{dt} = (C_{i,blood} - C_{i,perfusate})\frac{F_{perfusate}}{V_{perfusate}} \tag{5.3}$$

$C_{i,perfusate}$ - concentration of metabolite i in the perfusion medium (µmol / ghep).
$V_{perfuate}$ - volume of the perfusion medium.
$F_{perfusate}$ - perfusate flow rate through the liver.
$J_{i,b-t}$ - transport rate between the blood and tissue domains, (µmol / ghep min)
$R_{i,j}$ - is the reaction rate of each reaction j with metabolite i as substrate or product

Eq (5.1) and (5.2) are written only for those metabolites which are expected to occur in blood (i.e. GLC, LAC, ALA, AcAc, BHB, PYR). The perfusion medium vessel is also considered as well mixed system. The quantities $F_{perfusate}$ and $V_{perfusate}$ in Eqn. (5.1) are assigned values that match the specific experimental conditions from the literature.

The rate mechanism for transport between the blood and tissue domains is described by facilitated diffusion. Reversible near-equilibrium reactions (e.g. $R_{GAP \rightarrow PEP}$, R_{LDH}) are represented by a simplified form of a reversible, ping-pong mechanism, with the Haldane equation used to relate kinetic parameters values at near-equilibrium and to ensure consistency with thermodynamic constraints. The kinetic parameters were generally obtained either from *in vitro* kinetic studies with purified enzymes, by calculation from in vivo data and the assumed rate expression, or a combination of these methods.

Redox ratios are significantly different in cytosolic and mitochondrial compartments. Accounting for this difference is extremely important especially for investigating effect of ethanol metabolism, since both the reactions for ethanol removal involves NAD^+ and NADH as substrate and product. We tried to address this issue by establishing a pseudo-mitochondrial compartment for NADH/NAD^+, with the assumption that the mitochondrial redox ratio, RSm (defined as $C_{NADH(M)}$ / $C_{NAD^+(M)}$), is in equilibrium with the cytosolic ratio RS ($C_{NADH(C)}$ / $C_{NAD^+(C)}$); this assumption is expressed as $RS_m = K_{eq,RS} \cdot RS$. The equilibrium constant $K_{eq,RS}$ is calculated from the ratios of free cytosolic and mitochondrial C_{NADH} /C_{NAD^+} at the fasted steady state, obtained from measurements of C_{LAC} / C_{PYR} and C_{BHB}/C_{AcAc}, respectively, at equilibrium [38, 55, 58].

Chapters III and IV describe individual kinetic models for important regulatory steps like PFK – FBPase with their independent validation. For complete list of all the kinetic models used in the lumped model along with their constants, please refer the appendix of this thesis.

The lumped model with ethanol metabolism thus consist a total of 66 fluxes which include transport and kinetics, 39 concentration terms of metabolites in blood, tissue and perfusate and as a result 39 ordinary differential equations for mass balances. The code was originally written in FORTRAN. As part of this thesis work, the code was converted to MatLab and the 39 mass balances were solved simultaneously using MatLab ordinary differential equation solver ode15s. We selected ode15s based on the understanding of stiffness of the system, recognized during previous simulation runs on FORTRAN.

5.2 Simulation Method

In this section results from the lumped model with infusion of ethanol metabolism are discussed and compared to literature data.

Krebs [35, 36, 37] performed experiments with perfused rat liver to study the effect ethanol on gluconeogenesis from lactate. The data published in Krebs et al (1969) [35] is compared to the calculated results. In these experiments, he estimated the rate of glucose formation at different initial ethanol concentrations and 10 mM initial lactate as the recirculating single infusion. Accordingly, we set the initial concentration of lactate in perfusion to 10 mM and the program was run using 6 different concentrations of ethanol in the perfusion medium used by Krebs, shown in Table V. The initial conditions used for other metabolites are shown in Table VII. These metabolite concentrations are

from the initial lumped model without ethanol metabolism, validated with the data obtained from Williamson et al [67].

The simulation is run over a time span of 0 to 130 min. Lactate and ethanol perfusion begins at time t = 0 min. A single dose (pulse) of both substrates is added over the entire time span. The recirculating perfusion method used is described [35]. Seven separate sets of initial conditions were prepared. In each data set all the metabolite concentrations are same except ethanol, which is increasing from 0 to 40, as used by Krebs in his experiments. All these seven initial conditions are simulated separately, each generating a comprehensive set of metabolite concentrations and fluxes with respect to time. For this purpose a main MatLab program is written which can accept all these initial conditions and run ode15s for each condition, solving 39 ordinary differential equations for the mass balances along with their kinetic and transport equations for each particular time step. A time-average over the simulated time span is calculated for all the fluxes, similar to the method reporting in Krebs' paper.

Table VI Ethanol and lactate concentrations added in perfusate for different initial conditions used in simulation.

Experiment No.	Initial Ethanol concentration in perfusion medium mM	Initial lactate concentration in perfusion medium mM
1	0	10
2	1.25	10
3	2.5	10
4	5	10
5	10	10
6	20	10
7	40	10

Table VII Other initial metabolite concentrations used, common to all initial conditions of (Table VI).

Metabolite	Concentration in µmol/ghep	Metabolite	Concentration in µmol/ghep
Glcucose_blood	0.46	Alanaine _blood	0
Glcucose_tissue	0.47	Acetoacetate_tissue	0.82
Lactate_blood	0	BHB	0.15
Lactate_tissue	0	Pyruvate_blood	0
G6P	0.001	Acetoacetate _blood	0.80
Glycogen	108.01	BHB_blood	0.14
ATP	1.00	NH4	0.58
NADH	0.0001	F6P	0.0006
Pyruvate	0	F16BP	0.0007
AcCoA	0.009	Glcucose_perfusate	0.45
PEP	0	Acetoacetate _ perfusate	0.75
GAP	0	BHB_ perfusate	0.14
FFA	0.07	Etoh_blood	0
TG_tissue	3.74	Etoh_tissue	0
GLR_tissue	0	Acetaldehyde	0
GR3P	0	Acetate_blood	0
FFA_blood	-0.018	Acetate_tissue	0
GLR_blood	0.05		
TG_blood	0		
Alanaine_tissue	0.17		

5.3 Results

Figure 10 (A) shows the flux of the reaction catalyzed by alcohol dehydrogenase for the initial conditions of different ethanol concentrations as shown in the Table VI and VII. It can be observed that the flux decreases around ethanol concentration 10mM. This shows the important feature of the Theroll – Chance mechanism: the ethanol substrate inhibition at high concentration (≤ 10 mM), discussed in Chapter IV. Numerous authors, including Krebs, have pointed out this characteristic behavior of alcohol dehydrogenase [35, 43, 44].

Figure 10 (B) shows the flux of the reaction catalyzed by aldehyde dehydrogenase for the initial conditions (X-axis) used at different ethanol concentrations as shown in Table VI. The substrate acetaldehyde is produced from the oxidation of ethanol; as a result, the flux of aldehyde dehydrogenase reaction also shows similar trend as alcohol dehydrogenase, shown in Figure 10 (A). Figure 10 (C) shows the rate of NADH production. Since the change in the redox production rate is also triggered by oxidation of ethanol. A similar trend can be observed by means NADH production.

Figure 10 (D), (E) and (I) show the net transport of ethanol and acetate from blood to tissue. It can be observed that around 60 to 72% of the ethanol uptake by the tissue is transported back into the blood as acetate. This is in agreement with experimental results of 60 to 73% [53, 69]. Thus, only a small part of acetate is converted in to acetyl CoA, while most of acetate is transported back into blood. This characteristic is attributed to the fact that the high concentration of NADH produced during ethanol metabolism strongly inhibits the enzymes the citric acid cycle: isocitrate dehydrogenase and α-ketoglutarate dehydrogenase. [60, 61]

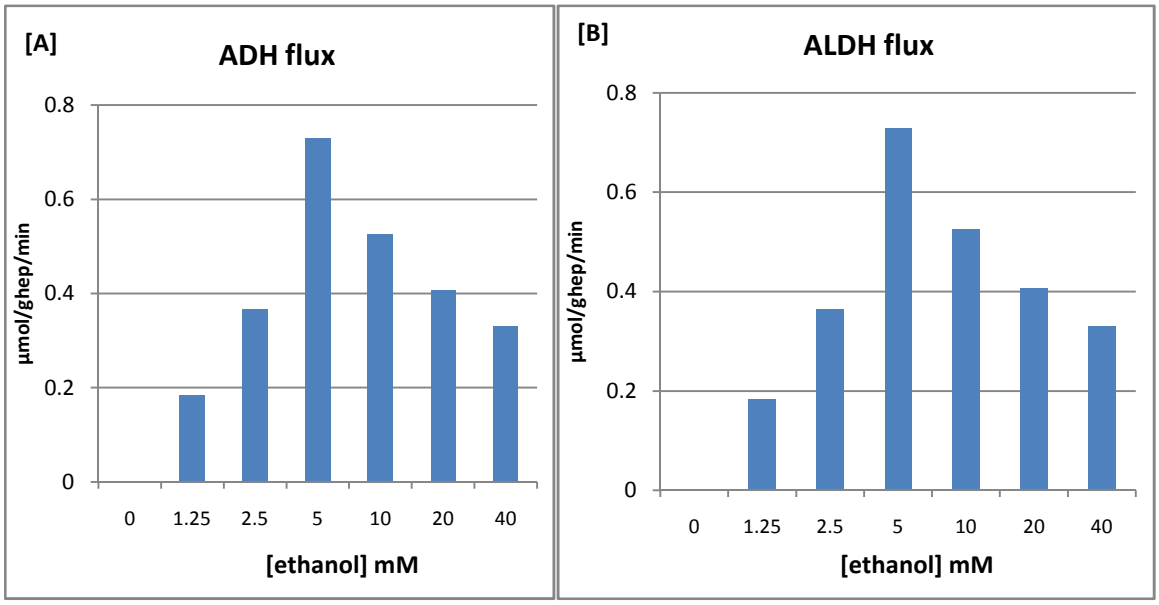
[A]
ADH flux
0.8
0.6
0.4
0.2
0
µmol/ghep/min
0
1.25
2.5
5
10
20
40
[ethanol] mM
[B]
ALDH flux
0.8
0.6
0.4
0.2
0
µmol/ghep/min
0
1.25
2.5
5
10
20
40
[ethanol] mM

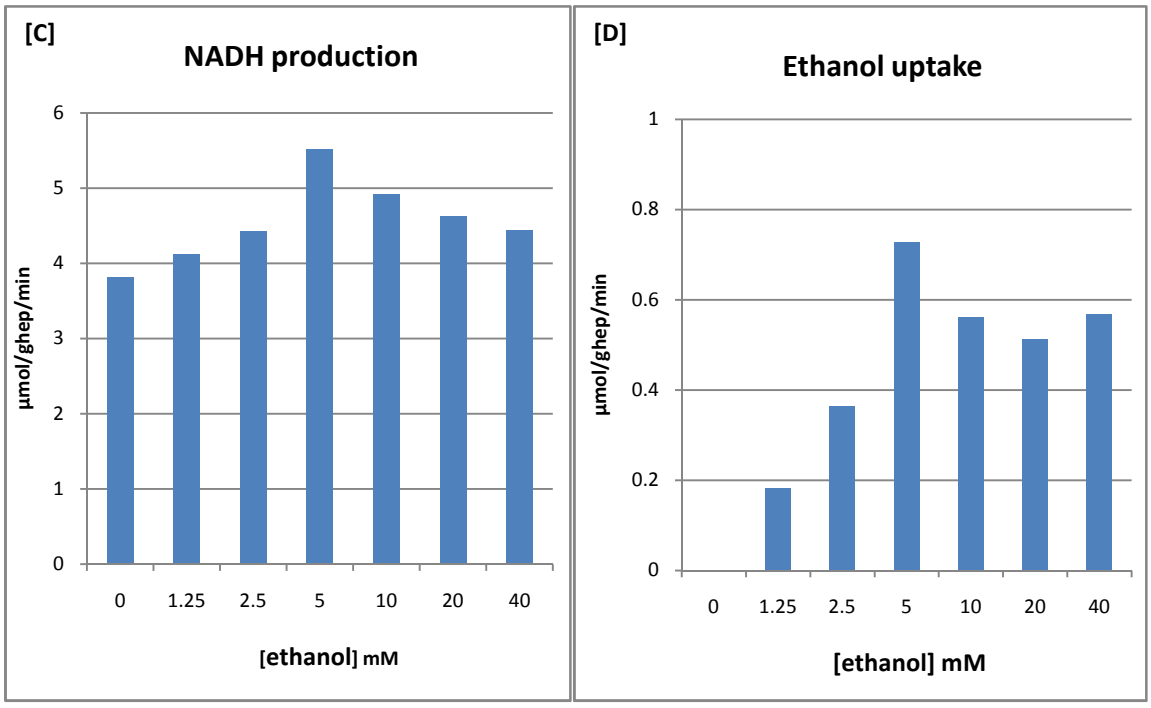
[C]
NADH production
6
5
4
3
2
1
0
µmol/ghep/min
0
1.25
2.5
5
10
20
40
[ethanol] mM
[D]
Ethanol uptake
1
0.8
0.6
0.4
0.2
0
µmol/ghep/min
0
1.25
2.5
5
10
20
40
[ethanol] mM

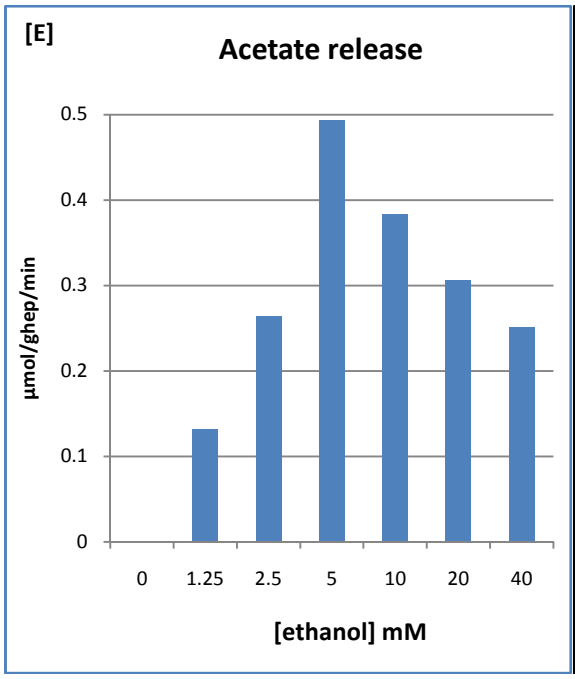
[E]
Acetate release
µmol/ghep/min
0.5
0.4
0.3
0.2
0.1
0
0
1.25
2.5
5
10
20
40
[ethanol] mM

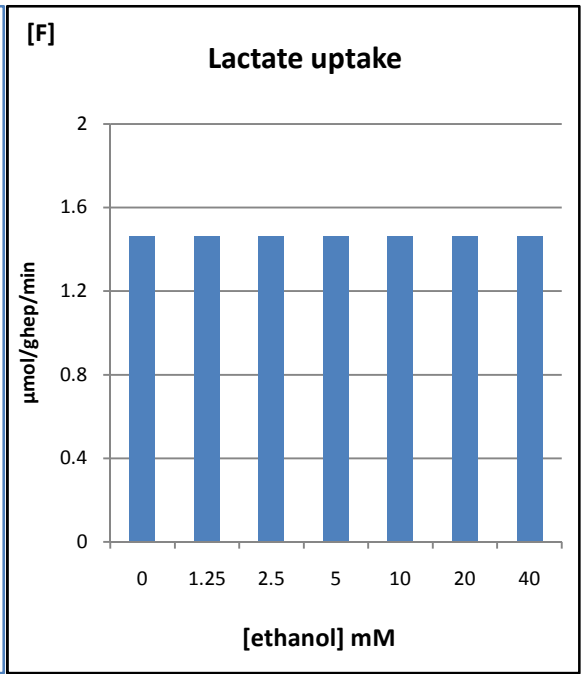
[F]
Lactate uptake
µmol/ghep/min
2
1.6
1.2
0.8
0.4
0
0
1.25
2.5
5
10
20
40
[ethanol] mM

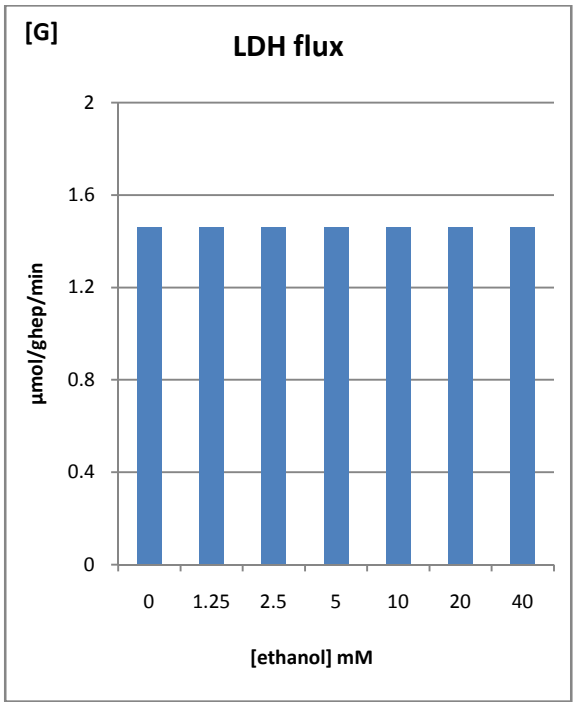
[G]
LDH flux
µmol/ghep/min
2
1.6
1.2
0.8
0.4
0
0
1.25
2.5
5
10
20
40
[ethanol] mM

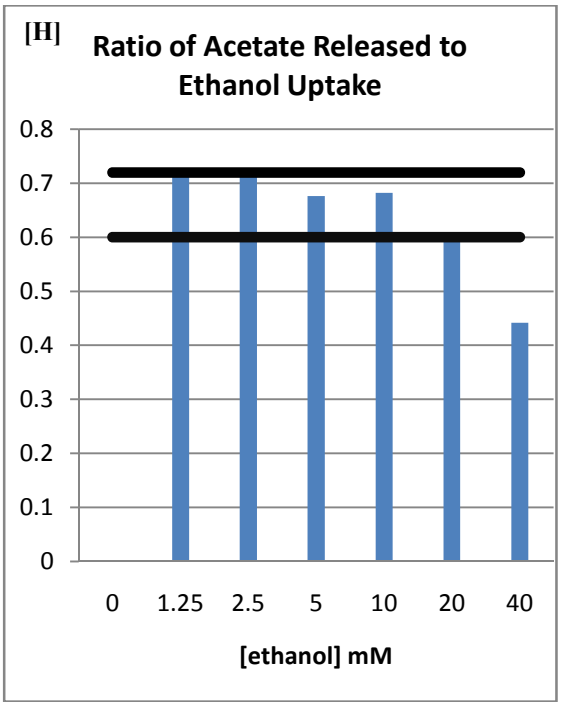
[H]
Ratio of Acetate Released to Ethanol Uptake
0.8
0.7
0.6
0.5
0.4
0.3
0.2
0.1
0
0
1.25
2.5
5
10
20
40
[ethanol] mM

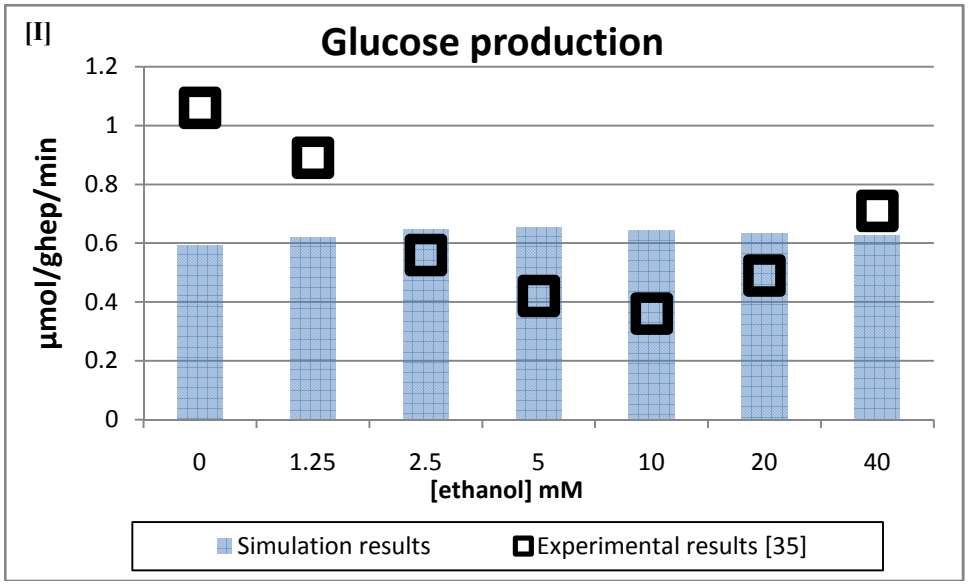

Figure 10 Simulation results for the lumped model of liver metabolism with ethanol. Weighted average of the flux over the time span 0 to 130 minutes is shown for each initial condition mentioned in Table VI for different ethanol concentration. Figure [H] show the ratio of flux of acetate released to the ethanol uptake, two horizontal lines show the experimental range reported in Huang et al, [69]. Figure [I] show the comparison of simulation results (bar) with experimental data (squares) from Krebs et al, [35].

Figure 10 (F) and (G) show the lactate uptake and the flux of the lactate dehydrogenase reaction for different initial conditions shown in Table VI. No change was observed in the simulation results of both these fluxes, which actually is contrary to the expected results. Since lactate to pyruvate is a reversible reaction converting one NAD^+ to one NADH, it is expected that as NADH concentration increases, the lactate dehydrogenase reaction is driven towards lactate, converting more pyruvate into lactate.

Finally, Figure 10 (I) shows the rate of glucose production along with the experimental data from Krebs. It can be observed that, even though the experimental results and the calculated values are in the same range, the main characteristic of ethanol metabolism inhibition of gluconeogenic flux in the fasted state, is actually missing. On the contrary, simulation results show a slight increase in the glucose production for the

initial ethanol concentration of 1.25, 2.5 and 5 mM. These apparent shortcoming are discussed in the next section.

To address these inadequacies we performed manual parameter estimation for the two important regulatory steps: reaction catalyzed by the enzyme pyruvate carboxylase and conversion of PEP to GAP. The basis for selection of these two reactions is the fact that both these reactions appreciably affect gluconeogenic fluxes and are significantly influenced by the change in the redox ratios. The intention was to check the effect of changes in the kinetic parameters of these regulatory steps on the average rate of glucose production. The selection of the kinetic parameters from those two reactions was based on their ability to alter sensitivity to redox ratios and the extent of initial approximation in the model (those estimated using *in vitro* data). For the same ethanol concentrations and simulation conditions the results are obtained by reducing the kinetic constant values by 10%, 50% and 90%. Results of this manual parameter estimation are shown in Figure 11 (A), (B) and (C). It can be observed that decreasing the maximum rate of the pyruvate carboxylase reaction, decreases the average glucose production for all initial conditions. This effect is significant if the Vmax is decreased to the 10% of its original value. But the required characteristic of inhibition of gluconeogenic flux is not obtained. Changes in kinetic constants for PEP to GAP reaction show only negligible effects on glucose production flux.

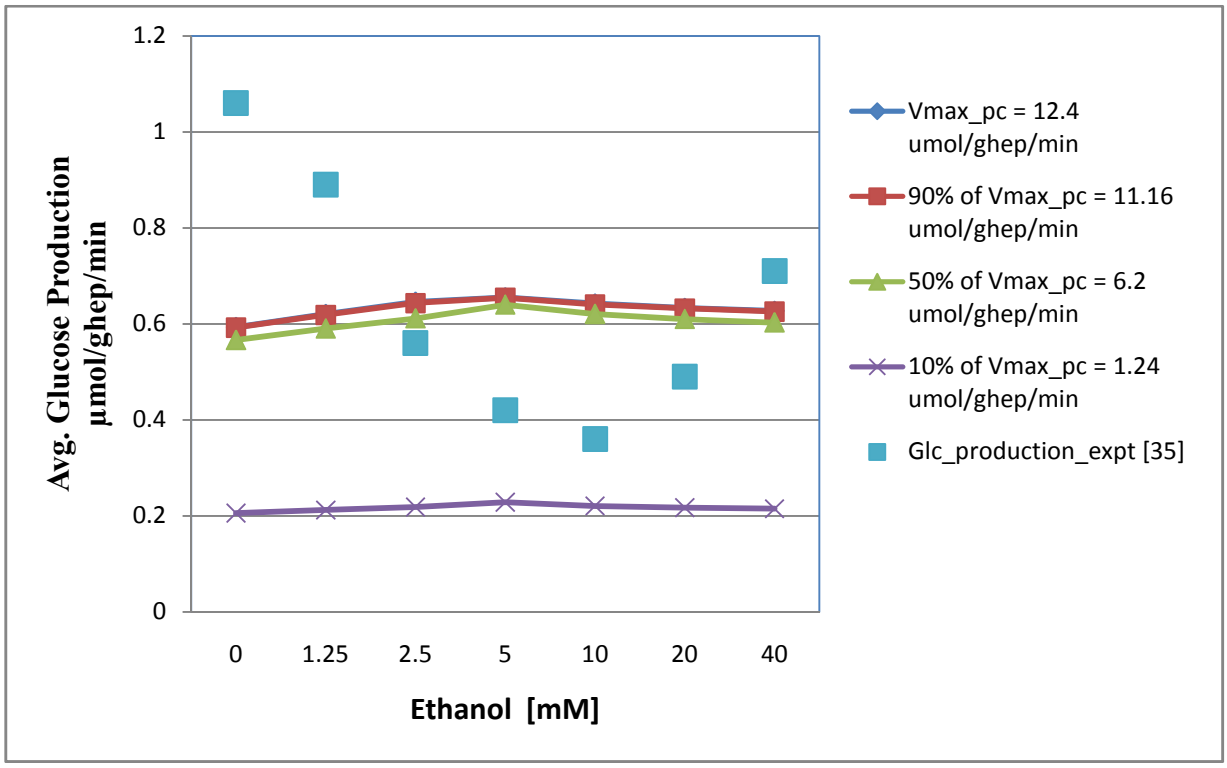

Figure 11 (A) Effect of change in Vmax_PC on glucose production flux [35].

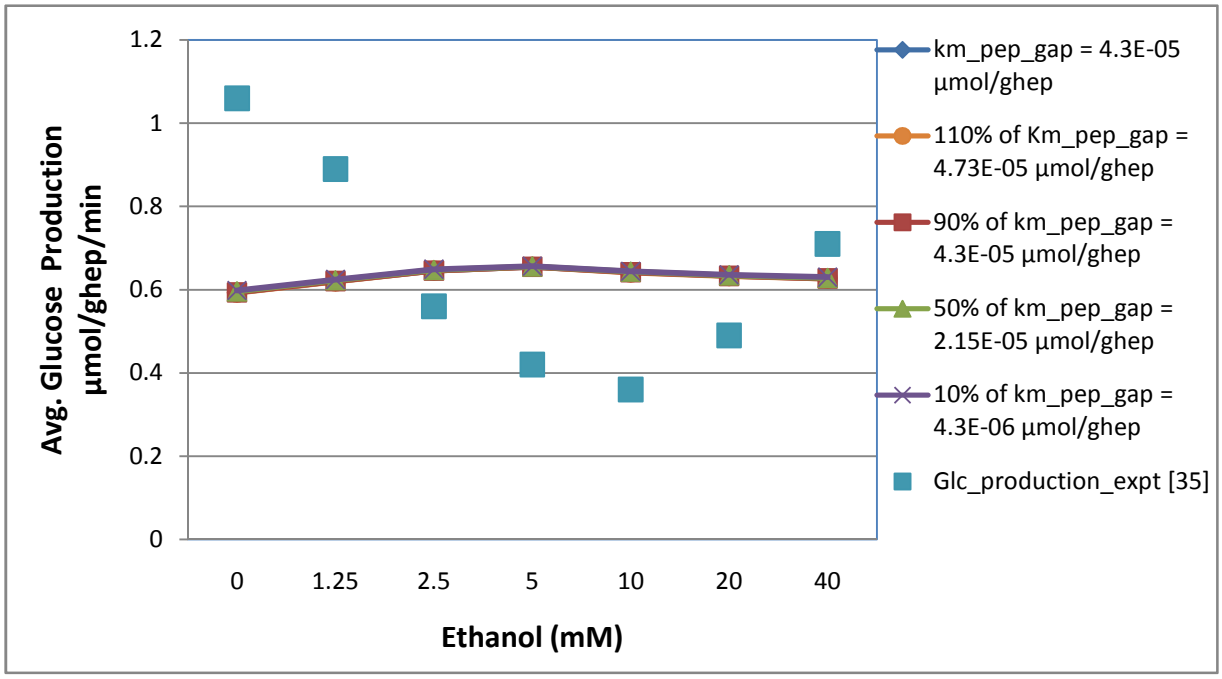

Figure 11 (B) Effect of change in Km_pep_gap on glucose production flux [35].

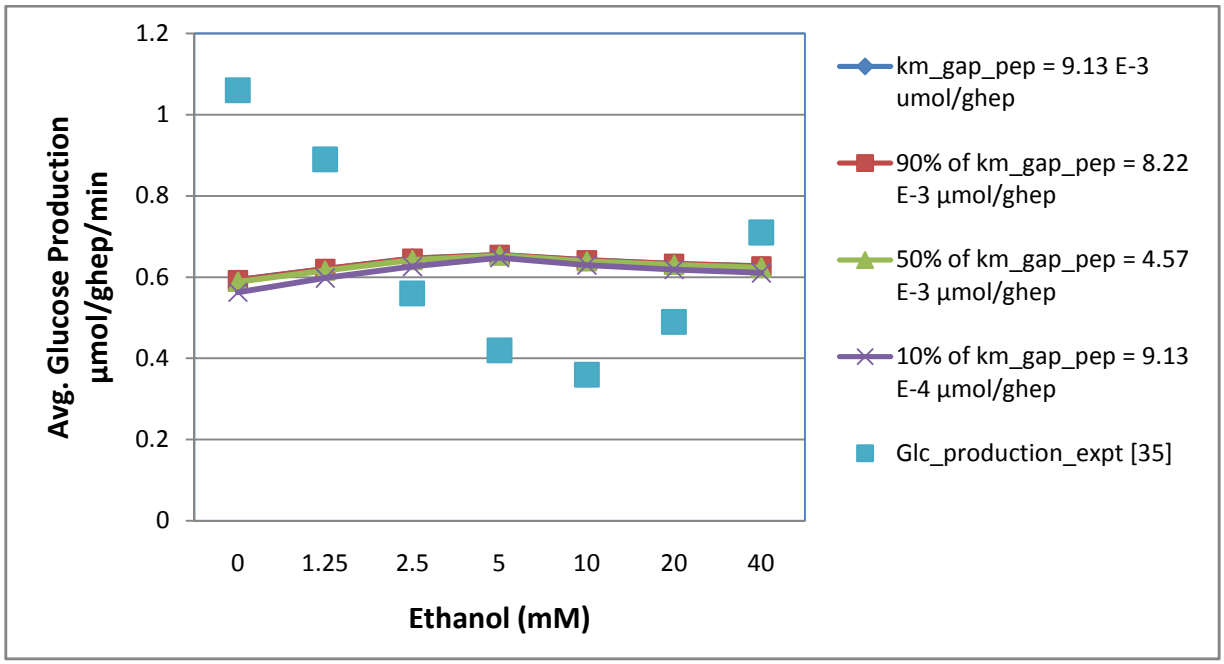

Figure 11 (C) Effect of change in Km_gap_pep on glucose production flux [35].

Figure 11 Effect of selected kinetic constants on simulation results of glucose production.

5.4 Discussion

The effect of ethanol metabolism on gluconeogenesis has been extensively studied in literature. Most of the experiments estimated rates of glucose production from various precursors such as alanine, glycerol, dihydroxy acetone, proline, galactose, fructose and so forth [36, 39, 40, 57]. The initial lumped model (before addition of ethanol metabolism part) was developed and validated considering the perfusion of lactate to estimate the rate of glconeogenesis based on data published by Williamson et al [67]. Accordingly, the basic aim of this thesis was to investigate the effect of ethanol metabolism on gluconeogenesis from lactate. A redox imbalance results from the oxidation of ethanol and acetaldehyde. On one hand high concentration of lactate drives the LDH reaction towards pyruvate, also converting one NADH into one NAD^+. On the other hand the higher rate of NADH production from alcohol dehydrogenase drives pyruvate towards lactate. Consequently, interpreting which of the control mechanism is superior is difficult.

As a result, starting from lactate only as a substrate source, it becomes very difficult to analyze and mathematically demonstrate the effect of ethanol on gluconeogenesis. Unfortunately, the data available for our specific application is scarce. Our results show almost no change in the lactate dehydrogenase flux and lactate uptake with increasing concentration of ethanol. These results can be largely ascribed to the fact that the model developed for the lactate dehydrogenase is not sensitive enough to changes in redox ratios produced by ethanol metabolism at high lactate concentration (10 mM).

Additional shortcoming of this effort has been the contradiction of calculated results with the experimental results that show inhibited rate of glucose production by

ethanol. These numerical results can be attributed to the two steps in gluconeogenic pathway: 1) the conversion of pyruvate to phosphoenolpyruvate (PEP) and 2) the conversion of phosphoenolpyruvate to glyceraldehyde-3-phosphate (GAP). In the current lumped model the conversion of pyruvate to PEP is represented by a lumped reaction catalyzed by enzyme pyruvate carboxylase. While this is a reasonable approximation to attain simplicity, while keeping the *in vivo* behavior achievable, in reality pyruvate is converted to oxaloacetate by pyruvate carboxylase and oxaloacetate is converted to PEP by enzyme PEPCK. Oxaloacetate is also part of citric acid cycle in which it is converted to malate by the enzyme malate dehydrogenase. Furthermore, oxaloacetate is the highly important part of malate aspartate shuttle, which ultimately is responsible for reoxidation of NADH to NAD^+ through the electron transport chain. Thus it can be concluded that in the presence of ethanol it is difficult to lump the reaction for conversion of pyruvate to PEP, neglecting further regulation of PEPCK and malate dehydrogenase.

The reaction catalyzed by pyruvate carboxylase is a highly important step in gluconeogenesis. Flux of this reaction is strong function of pyruvate concentration. In the presence of ethanol, lactate dehydrogenase reaction is inhibited because of high accumulation of NADH and pyruvate produced from lactate dehydrogenase reaction is extremely small. As a result, pyruvate carboxylase reaction is inhibited. Furthermore, as pyruvate carboxylase reaction is inhibited no oxaloacetate is produced. Thus complete malate – aspartate shuttle along with the electron transport chain is stopped. Because of all these effects NADH reoxidation is not possible which further increases the inhibition of all these reactions and ultimately inhibits the gluconeogenic flux. Figure 12 shows the

reoxidation of NADH through malate dehydrogenase shuttle in the mitochondrial compartment with the electron transport chain.

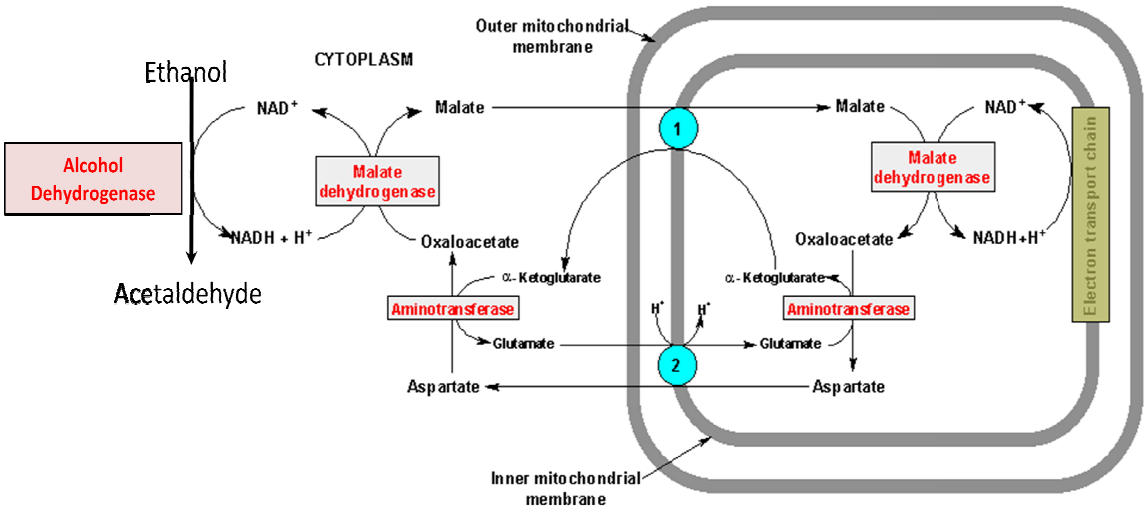

Figure 12. Electron transport chain for reoxidation of NADH with malate dehydrogenase shuttle[66].

Since the conversion of PEP to GAP is coupled with the oxidation of NADH to NAD^+, at high concentration of NADH the flux of PEP to GAP reaction increases, resulting in increased flux of glucose production. Thus an increased flux through PEP to GAP is triggered by the higher concentration of NADH, is shown in Figure 10 (I).

Currently the lumped model is constructed in two well mixed domains: blood and tissue. But in reality the intracellular compartmentation plays a vital role in cell metabolism. Acetaldehyde dehydrogenase reaction, the malate – aspartate shuttle responsible for NADH reoxidation, the complete TCA cycle including oxaloacetate reactions and the oxidative phosphorylation are the major controlling processes influenced by compartmentation. We have tried to establish a pseudo compartmentation using different NAD^+ and NADH concentrations, but it was not enough to correctly

simulate *in vivo* behavior. Establishing a formal mitochondrial compartment for appropriate metabolites and reactions along with the regulations of oxidative phosphorylation is important to analyze ethanol metabolism.

Irrespective of all these inadequacies, this thesis correctly shows the alcohol dehydrogenase flux characteristics. The complete lumped model based on the kinetic models developed for PFK, FBPase, ADH, ALDH and other enzymes predicts the glucose production fluxes within the range of experimental results. This achieves the first and foremost important step in establishing a framework for modeling fundamental regulation of the liver metabolism. The shortcomings from the model are perceptible and can be addressed in future work to bring the model one step closer to reality.

CHAPTER VI

CONCLUSION

Lack of strong metabolic regulation for ethanol is attributed to the fact that ethanol is not formed in mammalian tissue and nor it is present in any of the natural resources of food. Still the effect of ethanol on metabolic system is severely deteriorating. Our attempt has been not only to bring serious attention to these issues, but also to present a practical option of using mathematical model to help address these issues in a realistic way.

The kinetic models developed for the substrate cycle through PFK and FBPase are acceptable quantitative description of *in vitro* experimental data and are based on the latest findings on the enzymes. Even though the constants of these two models are not uniquely estimated, the expected *in vivo* characteristics of the two enzymes were demonstrated in the simulation results.

The lumped model presented in this thesis predicts the flux of glucose production in the correct range as compared to the experimental estimations by Krebs. Two important weaknesses can be identified from the results obtained; the model does not show expected inhibition of gluconeogenic pathway and the lactate uptake along with the lactate dehydrogenase flux remain unchanged for different ethanol concentrations.

Kinetic models for lactate dehydrogenase and pyruvate carboxylase can be further improved to obtain important regulatory characteristics of these enzymes exhibited at high NADH concentration during ethanol metabolism. It can be easily noticed that most of the alterations produced by ethanol are due to the changes in the redox ratios (to some extent accumulation of acetyl CoA is also responsible). Consequently the model can be further improved to a great extent by introducing a formal compartment for mitochondria and kinetics of malate dehydrogenase. This will allow us to account for the differential concentration and fluxes of metabolites across the mitochondrial membrane and enforce the necessary regulation of redox and the electron transport chain to influence the gluconeogenic fluxes. Once this model with mitochondrial compartment is established with appropriate validation, it can be used to study effect of ethanol on ketone body synthesis and fatty acid production.

With the recommended improvements to the model the simulated hepatic glucose production at different ethanol concentration can be easily related to hypoglycemia caused by alcoholism as well as other alcoholic liver disease. Thus importance of this effort of modeling ethanol metabolism cannot be overstated.

REFERENCES

PFK – FBPase Substrate Cycle:

1) Van Schaftingen E. & Hers, H. G. Control of liver 6-phosphofructokinase by fructose-2,6-bisphosphate and other effectors (1981) Proc. Natl. Acad. Sci. U.S.A. 78, 3483-86

2) Pilkis, S. J., El-Maghrabi, M. R., Pilkis, J. & Claus, T. Inhibition of fructose-1,6-bisphosphatase by fructose-2,6-bisphosphate. (1981a) J. Biol. Chem. 256, 3619-22

3) Meek, D. W. & Nimmo, H. G. The allosteric properties of rat liver fructose-1,6bisphosphatase. (1984) Biochem. J. 222, 125-30

4) Franqois, J., Van Schaftingen, E., Hers, H. G. On the mechanism of inhibition of neutral liver fructose-1,6-bisphosphatase by fructose-2,6-bisphosphatase. (1983)Eur. J. Biochem. 134, 269-73

5) McGrane, M. M., El-Maghrabi, M. R., Pilkis, S. J. The interaction of fructose-2,6-bisphosphate and amp with rat hepatic fructose 1,6-bisphosphatase. (1983) J. Biol. Chem. 258, 10445-54

6) Brand I. A., Soling H.D., Rat liver phosphofructokinase. purification and characterization of its reaction mechanism. J. Biol. Chem., (1974) 249, 7824-31

7) Ekdahl, K. N. Study on the regulation of rat liver pyruvate kiinase and fructose-1,6-bisphosphatase. (1987) Upsala J. Med. Sci. 92,217-32

8) Vidal, H., Roux B. & Riou. J. P. Phosphorylation and ligand induced conformational changes of rat liver fructose-1,6-bisphosphatase. (1986) Arch. Biochem. Biophy. 248, 604-11

9) Claus T. H., El-Maghrab M., PilkisS. J. The role of fructose-2,6-bisphosphatase in the regulation of carbohydrate metabolism. (1984) Curr. Top. Cell. Regu. 23, 57-86

10) Van Schaftingen, E. & Hers, H. G. Inhibition of fructose-1,6-bisphosphatase by fructose 2,6-biphosphate. (1981) Proc. Natl.Acad. Sci. U.S.A. 78, 2861-63

11) Pilkis, S. J., El-Maghrabi, M. R., Pilkis, J. & Claus, T. Inhibition of fructose-1,6-bisphosphatase by fructose 2,6-bisphosphate. (1981a) J. Biol. Chem. 256, 3619-22

12) Pilkis, S. J., El-Maghrabi, M. R., McGrane, M. M., Pilkis, J. & Claus, T. H. The role of fructose 2,6-bisphosphate in regulation of fructose-1,6-bisphosphatase. (1981b) J. Biol. Chem. 256, 11489-95

13) Hems D. A., Brosnan J.T. Effects of ischaemia on content of metabolites in rat liver and kidney in vivo. (1970) Biochem. J. 120, 105-11

14) Bergmeyer H. U., Methods of Enzymatic Analysis. 2nd Ed., Vol. 4, 2272-97

15) Segel I. H., Enzyme Kinetics. 1st Ed., 1975.

16) Reinhart, G. D., Hartleip, S. B., Influence of fructose 2,6 bisphosphate and MgATP on rat liver phosphofructokinase at ph 7: evedence for complex interdependence (1992) Arch. Biochem. Biophy. 296, 224-30

17) Uyeda, K., Furuya, E., Luby, l. J. The effect of natural and synthetic d-fructose 2,6 bisphosphate on the regulatory kinetic properties of liver and muscle phosphofructokinase
(1981) J. Biol. Chem. 256, 8394-99

18) Garfinkel, L., Kohn, M. C., Garfinkel, D., Computer simulation of the fructose bisphosphatase / phosphofructokinase couple in rat liver. (1978) J. Biochem. 96, 183-92

19) Ceppi, E. D., Knowels, R. G., Carpenter K. M., Effect of treatment of rats with bacterial endotoxin on fructose-2,6-bisphosphate metabolism and L-pyruvate kinase activity and flux in isolated liver cells. (1992) Biochem. J, 284, 761-66

20) Ekdahl K N., Ekman P., The effect of fructose-2,6-bisphosphaate and AMP on the activity of phosphorylated and unphosphorylated fructose-1,6-bisphosphatase from rat liver. (1983) FEBS, 167,2, 203-209

21) Veech, R. L., Kerbs, H. A., Cytosolic phosphorylation potential (1979) J. Bio. Chem., 254, 6538-47

22) Underwood A. H., Newsholme E., Properties of phosphofructokinase from rat liver and their relation to the control of glycolysis and gluconeogenesis. (1965) Biochem J. 95, 868-75.

23) W. Bartley, B. Dean, C. B. Taylor and E. Bailey., The effect on some enzymes of rat tissue of diets low in fat content. Biochem. J., (1967) 103, 2, 550 – 55

24) Crawford J M, Blum J J., Quantitative analysis of flux along the gluconeogenic, glycolytic and pentose phosphate pathways under reducing conditions in hepatocytes isolated from fed rats. Biochem J. (1983) 212, 3, 585-98

25) Rabkin M, Blum JJ., Quantitative analysis of intermediary metabolism in hepatocytes incubated in the presence and absence of glucagon with a substrate mixture containing glucose, ribose, fructose, alanine and acetate. Biochem J. (1985) 225, 3, 761-86.

26) Baranyai JM, Blum JJ., Quantitative analysis of intermediary metabolism in rat hepatocytes incubated in the presence and absence of ethanol with a substrate mixture including ketoleucine. Biochem J. (1989) 258, 1, 121-40.

27) Van Schaftingen E, Hue L, Hers HG., Study of the fructose 6-phosphate/fructose 1,6-bi-phosphate cycle in the liver in vivo. Biochem J. (1980), 192(1), 263-71

28) Hers H.G., Shaftingen V., The fructose 6-phosphste / fructose 1,6-bisphosphate cycle. Curr. Top. Cell. Reg. (1981) 18, 199-209

29) Van Schaftingen E, Hers HG., Fructose 2,6-bisphosphate 2 years after its discovery. Biochm. J. (1982) 206, 1-12

30) Reinhart GD, Lardy HA. Rat liver phosphofructokinase: kinetic activity under near-physiological conditions. Biochem.. (1980), 19(7), 1477-84

31) Jungermann, K., Heilbronn R., Katz N., Sasse D. The Glucose/Glucose-6-Phosphate Cycle in the Periportal and Perivenous Zone of Rat Liver. Eur. J. Biochem., (1982) 123, Issue 2, p429-436

32) Remesy C., Demigne C. Change in availability of gluconeogenic and ketogenic substrates and liver metabolism in fed or starved rats. Ann. Nutr. Metab (1983) 27, 57-70.

33) Chalhoub, E; L. Xie, V. Balasubramanian, J. Kim, J. Belovich A distributed model of carbohydrate transport and metabolism in the liver during rest and high-intensity exercise. Ann Biomed Eng. (2007), 35(3), 474-91.

34) Pilkis S. J. Claus T.H., Johanson R. A. Hormonal control of cyclic 3's'-amp levels and gluconeogenesis in isolated hepatocytes from fed rats, Bio. Chem. (1975) 250 (16) 6328-6336,

Ethanol Metabolism:

35) Krebs H. A., Freedland R. A., Hems R., Stubbs M. Inhibition of hepatic gluconeogenesis by ethanol. Biochem J. (1969), 112(1), 117–124.

36) Krebs H. A., Perkins J. R. The physiological role of liver alcohol dehydrogenase. Biochem J. (1970), 118(4), 635–644.

37) Krebs H. A, The effects of ethanol on the metabolic activities of the liver. *Adv Enzyme Regul* (1968), 6, 467 – 480.

38) Chalhoub E., Hanson R., Belovich J. M., A Computer Model of Gluconeogenesis and Lipid Metabolism in the Perfused Liver. Am J Physiol Endocrinol Metab. (2007) 0, [ahead of print]

39) Williamson J. R., Scholz R., Browning E. T., Thurman R. G. Metabolic Effects of Ethanol in Perfused Rat Liver. J. Biol.Chem, (1969), 244, 5044 – 5054.

40) Veech R. L., Guynn R., Veloso D. The time-course of the effects of ethanol on the redox and phosphorylation states of rat liver. Biochem J. (1972), 127(2), 387–397.

41) Plapp B. V., Leidal K.G., Smith R. K., Murch B. P. Kinetics of inhibition of ethanol metabolism in rats and the rate-limiting role of alcohol dehydrogenase. Arch Biochem Biophys. (1984), 230(1), 30-8.

42) Marjanen, L. Intracellular localization of aldehyde dehydrogenase in rat liver. Biochem J. (1972), 127(4), 633–639.

43) Crabb D. W., Bosron W. F., Li T. K. Steady-state kinetic properties of purified rat liver alcohol dehydrogenase: application to predicting alcohol elimination rates in vivo. Arch Biochem Biophys. (1983), 224(1), 299-309.

44) Bosron W. F., Crabb D. W., Li T. K. Relationship between kinetics of liver alcohol dehydrogenase and alcohol metabolism. Pharmacol Biochem Behav. (1983), 18(1), 223-7.

45) Umulis D. M., Gürmen N. M., Singh P., Fogler H. S. A physiologically based model for ethanol and acetaldehyde metabolism in human beings. Alcohol. (2005), 35(1), 3-12.

46) Svanas G. W., Weiner H. Aldehyde dehydrogenase activity as the rate-limiting factor for acetaldehyde metabolism in rat liver. Arch Biochem Biophys. (1985) 236(1), 36-46.

47) Parrilla R., Okawa K., Lindros K. O., Zimmerman U. J., Kobayashi K., Williamson J. R., Functional compartmentation of acetaldehyde oxidation in rat liver. J Biol Chem. (1974), 249(15), 4926-33.

48) Lumeng L., Bosron W. F., Li T. K., Quantitative correlation of ethanol elimination rates in vivo with liver alcohol dehydrogenase activities in fed, fasted and food-restricted rats. Biochem Pharmacol. (1979), 28(9), 1547-51.

49) Cornell N. W. Properties of alcohol dehydrogenase and ethanol oxidation in vivo and in hepatocytes. Pharmacol Biochem Behav. (1983), 18(l), 215-21.

50) Ehrig T., Bosron W. F., Li T. K. Alcohol and aldehyde dehydrogenase. Alcohol. (1990), 25(2-3), 105-16.

51) Mokuda O., Tanaka H., Hayashi T., Ooka H., Okazaki R., Sakamoto Y. Ethanol stimulates glycogenolysis and inhibits both glycogenesis via gluconeogenesis and from exogenous glucose in perfused rat liver. Ann Nutr Metab. 2004;48(4):276-80

52) Lumeng L., Bosron W. F., Li T. K., Rate-determining factors for ethanol metabolism in vivo during fasting. Adv Exp Med Biol. (1980), 132, 489-96.

53) Lindros K. O., Vihma R., Forsander O. A. Utilization and metabolic effects of acetaldehyde and ethanol in the perfused rat liver. Biochem J. (1972) 126(4), 945-52.

54) Petersen D. R., Collins A. C., Deitrich R. A. Role of liver cytosolic aldehyde dehydrogenase isozymes in control of blood acetaldehyde concentrations. J Pharmacol Exp Ther. (1977), 201(2), 471-81.

55) Cronholm T., NAD+-dependent ethanol oxidation: redox effects and rate limitation. Pharmacol Biochem Behav. (1983), 18(1) 229-32.

56) Haslett,Chilvers,Hunter,Boon. Davidson' s Principles and Practice of Medicine. 18th ed. Churchill Livingston. 1999

57) Crow K. E., Newland K. M., Batt R. D. Factors influencing rates of ethanol oxidation in isolated rat hepatocytes. Pharmacol Biochem Behav. (1983), 18, 237-40.

58) Ryle P. R., Chakraborty J., Thomson A. D. The roles of the hepatocellular redox state and the hepatic acetaldehyde concentration in determining the ethanol elimination rate in fasted rats. Biochem Pharmacol. (1985), 34(19), 3577-83.

59) Eriksson C. J. Increase in hepatic NAD level--its effect on the redox state and on ethanol and acetaldehyde metabolism. FEBS Lett. (1974), 40(2), 317-20.

60) Thurman R. G., McKenna W. R. Pathways of ethanol metabolism in perfused rat liver. Adv Exp Med Biol. (1975), 56, 57-76.

61) Thurman R. G, McKenna W. R, Brentzel H. J. Jr, Hesse S. Significant pathways of hepatic ethanol metabolism. Fed Proc. (1975), 34(11), 2075-81.

62) Handler J. A, Thurman R. G. Redox Interactions between catalase and alcohol dehydrogenase pathways of ethanol metabolism in the perfused rat liver. J Biol Chem. (1990), 265(3), 1510-5.

63) Teschke R, Hasumura Y, Lieber C. S. Hepatic microsomal alcohol-oxidizing system. Affinity for methanol, ethanol, propanol, and butanol. J Biol Chem. (1975), 250(18), 7397-404.

64) Lieber C. S. The discovery of the microsomal ethanol oxidizing system and its physiologic and pathologic role. Drug Metab Rev. (2004), 36(3-4), 511-29.

65) Yuki T, Thurman R. G. The swift increase in alcohol metabolism. Time course for the increase in hepatic oxygen uptake and the involvement of glycolysis. Biochem J. (1980), 186(1), 119-26.

66) Roberts B. J., Shoaf S. E., Jeong K. S., Song B. J. Induction of CYP2E1 in Liver, Kidney, Brain and Intestine During Chronic Ethanol Administration and Withdrawal: Evidence That CYP2E1 Possesses a Rapid Phase Half-Life of 6 Hours or Less. Biochem. and Biophy. Res. Commu. (1994), 205(2), 1064-1071

67) Williamson J. R, Browning E. T, Scholz R. Control mechanisms of gluconeogenesis and ketogenesis. I. Effects of oleate on gluconeogenesis in perfused rat liver. J Biol Chem. (1969), 244(17), 4607-16.

68) Carl A. Goresky and Brita E. Nadeau. Uptake of Materials by the Intact Liver: The exchange of glucose across the cell membranes. *The Journal of Clinical Investigation.* (1974), 53, 634-646.

69) Huang M. T, Huang C. C, Chen M. Y. In vivo uptake of ethanol and release of acetate in rat liver and GI. Life Sci. (1993), 53(10), 165-70.

APPENDIX

Table 1. Reaction rate stoichiometry, kinetic expressions, and parameter values used in the model. Definitions: $PS=C_{ADP}/C_{ATP}$; $RS_m=C_{NADH(m)}/C_{NAD(m)}^{+}$;
For details please refer Chalhoub et al. (2007)

Rate	Kinetic Expression	Parameter Values	Method of determining parameters
		Parameters common to several reactions: $PS_i=0.44$ $RS_i=0.2$	Set equal to steady state C_{ADP}/C_{ATP} Set equal to steady state $C_{NADH(m)}/C_{NAD^{+}(m)}$
A. Reaction Rates			
R_{GK} GLC + ATP → G6P+ ADP	$\frac{V_{max,\ GK}\ C_{GLC\_t}}{K_{m,GK}+C_{GLC\_t}}\left(\frac{1/PS}{1/PS_i+1/PS}\right)$	$V_{max,GK}=2.19$ µmol gww hep^{-1}min^{-1} $K_{M,GK}=6.25$ µmol/gww hep	Calculated from R_{GK} flux (from FBA, assuming 30% cycling) and steady state GLC concentration Set equal to steady state GLC concentration
R_{G6Pase} G6P→GLC	$\frac{V_{max,\ G6Pase}\ C_{G6P}}{K_{m,G6Pase}+C_{G6P}}$	$V_{max,G6Pase}=3.65$ µmol gww hep^{-1}min^{-1} $K_{m,G6Pase}=0.102$ µmol/gww hep	Calculated from R_{G6Pase} flux from FBA and steady state G6P concentration Set equal to steady state G6P concentration

R_{GI} G6P ↔ F6P	$\frac{\frac{V_{\max,G6P,GI}}{K_{m,F6P,GI}}\left(C_{F6P}-\frac{C_{G6P}}{K_{eq,GI}}\right)}{1+\frac{C_{F6P}}{K_{m,F6P,GI}}+\frac{C_{G6P}}{K_{m,G6P,GI}}}$	$V_{max,G6P,GI}$ =*32.8* µmol gww hep^{-1}min^{-1} $K_{m,F6P,GI}$ =*0.046* µmol/gww hep $K_{m,G6P,GI}$ =*0.10* µmol/gww hep $K_{eq,GI}$=*2.5*	Calculated from R_{GI} flux from FBA and steady state F6P and G6P concentrations Set equal to steady state F6P concentration Set equal to steady state G6P concentration Calculated from in vivo concentrations
R_{FBPase} F1,6BP → F6P	$\frac{V_{\max,FBPase}\frac{\mu(1+\mu)^{n_{fgbp}}}{(1+\beta)^{n_{fbp}}(1+\sigma)^{n_{fbp}}}(1+\beta\gamma+\delta\gamma)^{n_{fbp}}}{L_{FBP}\frac{\left(1+\beta^{n_{fbp}}\right)}{(1+c_{FBP}\gamma)^{n_{fbp}}}+(1+\mu)^{n_{FBP}}}$ $\mu=\frac{C_{F1,6BP}}{K_{F1,6BP,FBPase}};\beta=\frac{C_{F2,6BP}}{K_{iF2,6BP,FBPase}};$ $\gamma=\frac{C_{cAMP}}{K_{icAMP,FBPase}};\delta=\frac{C_{AMP}}{K_{iAMP,FBPase}}$	$V_{max,FBPase}$=*20* µmol gww hep^{-1}min^{-1} $K_{F1,6BP,FBPase}$=*4.84E-04* µmol/gww hep* $K_{icAMP,FBPase}$=*9.23E-03* µmol/gww hep* $K_{iF2,6BP,FBPase}$ =*1.56E-02* µmol/gww hep $K_{iAMP,FBPase}$=*0.106* µmol/gww hep n_{FBP}=*5.52* L_{FBP}=*2.76E+06* C_{FBP}=*0.56*	Calculated from in vitro kinetic data *modified 10- 20% from the original source.

R_{PFK} F6P + ATP → F1,6BP + ADP	$\frac{V}{V_{max,PFK}} = \frac{C_{ATP} \cdot C_{F6P}^{2}}{K_{PFK} + C_{ATP} \cdot C_{F6P}^{2}}$ $K_{PFK} = K_{F6P,PFK}^{APP}\left(\frac{C_{ATP} + K_{ATP,PFK} + T_1^{n1}\frac{C_{ATP}^{2}}{K_{iATP,PFK}}}{1 + T_2^{n2} + T_1^{n1}}\right)^{2}$ $T_1 = \alpha\left(\frac{K_{iF2,6BP,PFK} + C_{F2,6BP}}{K_{iF2,6BP,PFK} + Q1 \cdot C_{F2,6BP}}\right)$ $T_2 = \sigma\left(\frac{K_{iAMP,PFK} + C_{AMP}}{K_{iAMP,PFK} + Q2 \cdot C_{AMP}}\right)$	$V_{max,PFK}$=*3.75* µmol gww hep^{-1}min^{-1} $K_{ATP,PFK}$=*2.91E-02* µmol/gww hep $Ki_{ATP,PFK}$=*0.058* µmol/gww hep $Ki_{AMP,PFK}$=*1.16* µmol/gww hep $K^{APP}_{F6P,PFK}$=*4.0E-04* µmol/gww hep $Ki_{F2,6BP,PFK}$=*1.7E-02* µmol/gww hep *α =2.0* *σ=3.5* *n1=3.0* *n2=3.0* *Q1=100* *Q2=50*	Calculated from in vitro kinetic data.
R_{PK} PEP + ADP → PYR + ATP	$\frac{V_{max,PK}\pi(1+\pi+\gamma)^{n_{PK}-1}}{L_p\frac{(1+\beta)^{n_{pk}}(1+\kappa_{ATP,PK}\gamma)^{n_{PK}}}{(1+\kappa_{ALA,PK}\beta)^{n_{PK}}(1+\phi)^{n_{PK}}} + (1+\pi+\gamma)^{n_{PK}}}$ $\pi = \frac{C_{PEP}}{K_{PEP,PK}}; \gamma = \frac{C_{ATP}}{K_{ATP,PK}};$ $\beta = \frac{C_{ALA}}{K_{iALA,PK}}; \phi = \frac{C_{FBP}}{K_{FBP,PK}}$	$V_{max,PK}$=*62.5*µmol gww hep^{-1}min^{-1} $K_{PEP,PK}$=*3.2E-02* µmol/gww hep $K_{ATP,PK}$=*0.435* µmol/gww hep $K_{iALA,PK}$=*1.16E-01*µmol/gww hep $K_{FBP,PK}$=*5.80E-04* µmol/gww hep* L_p=*1.60E+04* n_{PK}=*3.10* $\kappa_{ATP,PK}$=*2.0* $\kappa_{ALA,PK}$=*0.2*	Calculated from in vitro kinetic data; modified from the original source.

R_{LDH} $LAC + NAD^+ \leftrightarrow PYR + NADH$	$\frac{\frac{V_{max,LDH}}{K_{m,LAC,LDH}}\left(C_{LAC}C_{NAD^+(c)} - \frac{C_{PYR}C_{NADH(c)}}{K_{eq,LDH}}\right)}{1 + \frac{C_{LAC}C_{NAD^+(c)}}{K_{m,LAC,LDH}} + \frac{C_{PYR}C_{NADH(c)}}{K_{m,PYR,LDH}}}$	$V_{max,LDH}$=*195* µmol gww hep^{-1}min^{-1} $K_{m,LAC,LDH}$=*1.43* µmol/gww hep $K_{m,PYR,LDH}$=*4.77E-05* µmol/gww hep $K_{eq,LDH}$=*1.1E-04*	in vitro Set equal to product of steady state LAC and $NAD^+(c)$ [a] concentrations Calculated from in vivo LDH flux[15] and steady state LAC, PYR, $NAD^+_{(c)}$[a], and $NADH_{(c)}$[b] concentrations in vitro
$R_{ALA \rightarrow PYR}$ $ALA + NAD^+ \rightarrow PYR + NADH$	$\frac{\frac{V_{max,ALA,PYR}}{K_{m,ALA,PYR}}\left(C_{ALA}C_{NAD^+(c)} - \frac{C_{PYR}C_{NADH(c)}}{K_{eq,ALA,PYR}}\right)}{1 + \frac{C_{ALA}C_{NAD^+(c)}}{K_{m,ALA,PYR}} + \frac{C_{PYR}C_{NADH(c)}}{K_{m,PYR,ALA}}}$	$V_{max,ALA,PYR}$=*300* µmol gww hep^{-1}min^{-1} $K_{mALA,PYR}$=*0.71* µmol/gww hep $K_{m,PYR,ALA}$=*2.4E-07* µmol/ gww hep $K_{eq,ALA,PYR}$=*2.5E-03*	in vitro Set equal to product of steady state ALA and $NAD^+(c)$[a] concentrations Calculated from in vivo flux[15] and steady state ALA, $NAD^+_{(c)}$[a] , PYR and NADH(c)[b] concentrations In vitro
$R_{PYR \rightarrow PEP}$ $PYR + ATP + GTP \rightarrow PEP + ADP + GDP + Pi + CO_2$	$\frac{V_{max,PC}\frac{1}{\left(1 + \frac{C_{ADP}}{K_{i,ADP,PYR,PC}}\right)}}{1 + \frac{K_{ATP,PC}}{C_{ATP}^{n_{1PC}}} + \frac{K_{PYR,PC}}{C_{PYR}^{n_{2PC}}\left(1 + \frac{C_{ADP}}{K_{i,ADP,PYR,PC}}\right)}\varpi}$ $\varpi = \left(\frac{1}{\left(1 + \frac{C_{AcCoA}^{n_{3PC}}}{K_{a,AcCoA,PC}}\right)} + \frac{K_{ATP}}{K_{i,ADP,ATP,PC}}\frac{C_{ADP}}{C_{ATP}^{n_{1PC}}}\right)$	$V_{max,PC}$=*12.4* µmol gww hep^{-1}min^{-1} $K_{ATP,PC}$=*0.034* (µmol/gww hep)^1.03 $K_{PYR,PC}$=*7.1* (µmol/gww hep)^0.8 $K_{iADP,PYR,PC}$=*1.74* µmol/gww hep $K_{iADP,ATP,PC}$=*0.521* µmol/gww hep $K_{a,AcCoA,PC}$=*2.28E-05* (µmol/gwwhep)^1.65 $n_{1,PC}$ =*1.03* $n_{2,PC}$ =*0.80* $n_{3,PC}$ =*1.65*	Calculated from in vitro kinetic data for pyruvate carboxylase

$R_{PEP \leftrightarrow GAP}$ PEP + ATP + NADH↔ GAP + ADP + NAD^+	$\frac{\frac{V_{max,PEP,GAP}}{K_{m,PEP,GAP}}\left(C_{PEP}C_{NADH(c)}C_{ATP}-\frac{C_{GAP}C_{Pi}C_{NAD(c)}C_{ADP}}{K_{eq,PEP,GAP}}\right)}{1+\frac{C_{PEP}C_{NADH(c)}C_{ATP}}{K_{m,PEP,GAP}}+\frac{C_{GAP}C_{Pi}C_{NAD(c)}C_{ADP}}{K_{m,GAP,PEP}}}$	$V_{max,PEP,GAP}$ =*94.0* µmol gwwhep^{-1}min^{-1} $K_{m,PEP,GAP}$ =*4.3E-05* µmol/gww hep $K_{m,GAP,PEP}$=*9.13E-03* µmol/ gww hep $K_{eq,PEP,GAP}$=*4166*	In vitro Set equal to product of PEP, NADH(c)[b], and ATP concentrations'; modified during parameter estimation Calculated from $R_{PEP \leftrightarrow GAP}$ flux from FBA and steady state PEP, ATP, NAD^+(c)[a], NADH(c)[b], GAP, and ADP In vitro
$R_{GAP \leftrightarrow F1,6BP}$ GAP↔F1,6BP	$\frac{V_{max,GAP,F1,6BP}C_{GAP}}{K_{m,GAP,F1,6BP}+C_{GAP}}$	$V_{max,GAP,F1,6BP}$ = *4.97* µmol gwwhep^{-1}min^{-1} $K_{m,GAP,F1,6BP}$ =*0.0194* µmol/gww hep	Calculated from $R_{GAP \leftrightarrow F1,6BP}$ flux from FBA and steady state GAP concentration Set equal to steady state GAP concentration[57,66]
R_{PDC} PYR + NAD^+ → AcCoA + NADH	$\frac{V_{max,PDC}C_{PYR}}{\left(1+\frac{\alpha_{PDC}}{PS}\right)\left(1+\beta_{PDC}\frac{C_{AcCoA}}{C_{CoA}}+\delta_{PDC}(RS_m)^2\right)(K_{PDC}+C_{PYR})}$	$V_{max,PDC}$ = *1.88* µmol gww hep^{-1}min^{-1} K_{PDC}=*0.20* µmol/gww hep $\alpha_{,PDC}$ = *0.9* $\beta_{,PDC}$ = *25;* $\delta_{,PDC}$ = *0.50*	Calculated from in vitro kinetic data
$R_{FFA \rightarrow AcCoA}$ FFA + 2ATP + $7NAD^+$ + 7FAD→ 8AcCoA + 7NADH + 7FADH + 2ADP	$\frac{V_{max,FFA,AcCoA}C_{FFA}}{K_{m,FFA,AcCoA}+C_{FFA}}\left(\frac{1/RS_m}{1/RS_i+1/RS_m}\right)\left(\frac{1/PS}{1/PS_i+1/PS}\right)$	$V_{max,FFA,AcCoA}$= 6.76 µmol gww hep^{-1}min^{-1} $K_{m,FFA,AcCoA}$ =0.36 µmol/gww hep	Calculated from in vivo flux**,** steady state FFA, PS, and RS_m concentrations Set equal to steady state FFA concentration

$R_{TG \rightarrow FFA}$	$\frac{V_{\max,TG,FFA} C_{TG,t}}{K_{m,TG,FFA} + C_{TG,t}}$	$V_{\max,TG,FFA}$ = 3.67 µmol gww hep^{-1}min^{-1} $K_{m,TG,FFA}$ =0.0071 µmol/ gww hep	Calculated from $R_{TG \rightarrow FFA}$ flux from FBA and steady state TG,t concentration Set equal to steady state TG,t concentration
$R_{GLR\_t \rightarrow GR3P}$ GLR+ATP→GR3P+ADP	$\frac{V_{\max,GLR,GR3P} C_{GLR,t}}{K_{m,GLR,GR3P} + C_{GLR,t}} \left(\frac{1/PS}{1/PS_i + 1/PS} \right)$	$V_{\max,GLR,GR3P}$ = 0.79 µmol gww hep^{-1}min^{-1} $K_{m,GLR,GR3P}$ = 0.125 µmol/ gww hep	Calculated from in vivo flux and steady state PS and assumed GLR,t concentrations. Set equal to the assumed steady state GLR,t concentration
$R_{GR3P \leftrightarrow GAP}$ GR3P+$NAD^+ \leftrightarrow$GAP+NADH	$\frac{\frac{V_{\max,GR3P,GAP}}{K_{m,GR3P,GAP}} \left(C_{GR3P} C_{NAD^+(c)} - \frac{C_{GAP} C_{NADH(c)}}{K_{eq,GR3P,GAP}} \right)}{1 + \frac{C_{GR3P} C_{NAD^+(c)}}{K_{m,GR3P,GAP}} + \frac{C_{GAP} C_{NADH(c)}}{K_{m,GAP,GR3P}}}$	$V_{max,GR3P,GAP}$= *115* µmol gww hep^{-1}min^{-1} $K_{m,GR3P,GAP}$=*0.47* µmol/gww hep $K_{m,GAP,GR3P}$=*7.06E-07* µmol/gww hep $K_{eq,GR3P,GAP}$=*1.3E-04*	in vitro Set equal to product of steady state GR3P and $NAD^+(c)$[a] concentrations Calculated from $R_{GR3P \leftrightarrow GAP}$ flux from FBA and steady state GR3P, $NAD^+(c)$[a], NADH(c)[b], and GAP concentrations In vitro

R_{FA_syn} $8AcCoA + 7ATP \rightarrow FFA_{c16} + 7ADP$	$\frac{V_{\max FA\_syn} C_{AcCoA}}{K_{m,FA\_syn} + C_{AcCoA}} \left(\frac{1/PS}{1/PS_i + 1/PS} \right)$	$V_{\max,FA\_syn}$ =2.7 µmol gww hep^{-1}min^{-1} K_{m,FA_syn}=0.13 µmol/gww hep	Calculated from R_{FA_syn} flux from FBA and steady state AcCoA concentration Set equal to the steady state AcCoA concentration.
R_{TG_f} $3FFA_{c16} + 2ATP + GR3P \rightarrow TG + 2ADP$	$\frac{V_{\max TG-f} C_{GR3P} C_{FFA}}{K_{m,TG-f} + C_{GR3P} C_{FFA}} \left(\frac{1/PS}{1/PS_i + 1/PS} \right)$	$V_{\max,TG-f}$ = 0.43 µmol gww hep^{-1}min^{-1} $K_{m,TG-f}$ =0.11 µmol/gww hep	Calculated from R_{TG_f} flux from FBA and steady state FFA concentration Set equal to the product of steady state FFA[14] and GR3P concentrations.
R_{TCA} $8AcCoA+ADP +3NAD^+ + FAD \rightarrow 16CO_2 + ATP + 3NADH +FADH$	$V_{mzx,TCA} C_{AcCoA} \left(\varepsilon \frac{1/RS_m}{1/RS_{i,} + 1/RS_m} + (1-\varepsilon) \frac{1/PS}{1/PS_{i,} + 1/PS} \right)$	$V_{max,TCA}$= *22.33* µmol gww hep^{-1}min^{-1} ε *=0.75*	Calculated from in vivo flux and steady state AcCoA concentration. Derived previously.
$R_{AcCoA \rightarrow AcAc}$ $2AcCoA \rightarrow AcAc+2CoA$	$\frac{V_{\max,AcCoA\_AcAc} C_{AcCoA}}{K_{m,AcCoA\_AcAc} + C_{AcCoA}}$	$V_{\max,AcCoA\_AcAc}$ = 9.28 µmol gww hep^{-1}min^{-1} $K_{m,AcCoA\_AcAc}$ =0.124 µmol/gwwhep	Calculated from $R_{AcCoA \rightarrow AcAc}$ flux from FBA and steady state AcCoA concentration
R_{BHBdh} $AcAc + NADH \leftrightarrow BHB + NAD$	$\frac{\frac{V_{\max,AcAc\_BHB}}{K_{m,AcAc\_BHB}} \left(C_{AcAc} C_{NADH(m)} - \frac{C_{BHB} C_{NAD^+(m)}}{K_{eq,BHBdh}} \right)}{1 + \frac{C_{AcAc} C_{NADH(m)}}{K_{m,AcAc\_BHB}} + \frac{C_{BHB} C_{NAD^+(m)}}{K_{m,BHB\_AcAc}}}$	$V_{\max,AcAc\_BHB}$ = 60 µmol gww hep^{-1}min^{-1} $K_{m,AcAc\_BHB}$ =0.0071µmol/ gww hep K_{m,BHB_AcAc} =0.0059µmol/ gww hep $K_{eq,BHBdh}$=20	In vitro Set equal to product of steady state concentrations of AcAc and $NADH_m$ (assumed = 0.01 µmol gww^{-1} hep) Calculated from R_{BHBdh} flux from FBA and steady state substrate concentrations in vitro

R_{OxPhos} $O_2 + 5ADP + 2NADH \rightarrow 2H_20 + 5ATP + 2NAD^+$	$\frac{V_{\max,OxPhos} C_{O_2}}{K_{m,OxPhos} + C_{O_2}} \left(\frac{PS}{PS + PS_i} \right) \left(\frac{RS_m}{RS_i + RS_m} \right)$	$V_{max,OxPhos}$= *37.8* µmol gww hep^{-1}min^{-1} $K_{m,OxPhos}$=*7.3* µmol/gww hep	Calculated from R_{OxPhos} flux from FBA and steady state O_2 concentration Set equal to the steady state O_2 concentration
R_{urea} $2NH_4+HCO_3+3ATP \rightarrow$ urea+2ADP+2Pi+AMP+PPi	$\frac{V_{\max,urea} C_{NH4}}{K_{m,urea} + C_{NH4}} \left(\frac{1/PS}{1/PS_i + 1/PS} \right)$	$V_{max,urea}$=*2.57* µmol gww hep^{-1}min^{-1} $K_{m,urea}$=*0.70* µmol/gww hep	Calculated from R_{urea} flux from FBA and steady state NH_4^+[7] concentration Set equal to steady state NH_4^+ concentration
$R_{Glyc \rightarrow G6P}$ $(Glyc)_n \rightarrow (Glyc)_{n-1}$ + G6P	$R_{Glyc \rightarrow G6P}$= 0.0358 µmol gww hep^{-1}min^{-1}		Set equal to in vivo flux
B. Transport Rates			
$J_{GLC,b-t,net}$	$\frac{V_{\max,Glc,b-t}(C_{Glc,b} - C_{Glc,t})}{(K_{m,Glc,b-t} + C_{Glc,b} + C_{Glc,t})}$	V_{max,Glc,b_t}= *17.8* µmol gww hep^{-1}min^{-1} K_{m,Glc,b_t}=*5.07* µmol/gww hep	Calculated from in vivo flux and steady state GLC,b concentration Set equal to steady state GLC,b concentration
$J_{LAC,b-t,net}$	$\frac{V_{\max,Lac,b-t}(C_{Lac,b} - C_{Lac,t})}{(K_{m,Lac,b-t} + C_{Lac,b} + C_{Lac,t})}$	V_{max,LAC,b_t}= *22.5* µmol gww hep^{-1}min^{-1} K_{m,LAC,b_t}=*1.2* µmol/gww hep	Calculated from in vivo flux and steady state LAC,b concentration Set equal to steady state LAC,b[15] concentration
$J_{FFA,b-t,net}$	$\frac{V_{\max,FFA,b-t}(C_{FFA,b} - C_{FFA,t})}{(K_{m,FFA,b-t} + C_{FFA,b} + C_{FFA,t})}$	V_{max,FFA,b_t}=*4.7* µmol gww hep^{-1}min^{-1} K_{m,FFA,b_t}=*0.67*µmol/gww hep	Calculated from in vivo flux and steady state FFA,b concentration Set equal to steady state FFA,b[15] concentration

$J_{GLR,b\text{-}t,net}$	$\frac{V_{max,GLR,b-t}(C_{GLR,b}-C_{GLR,t})}{(K_{m,GLR,b-t}+C_{GLR,b}+C_{GLR,t})}$	V_{max,GLR,b_t}= *2.53* µmol gww hep^{-1}min^{-1}	Calculated from in vivo flux and steady state GLR,b concentration
		K_{m,GLR,b_t}=*0.16* µmol/gww hep	Set equal to steady state GLR,b concentration
$J_{TG,b\text{-}t,net}$	$\frac{V_{max,TG,b-t}(C_{TG,b}-C_{TG,t})}{(K_{m,TG,b-t}+C_{TG,b}+C_{TG,t})}$	V_{max,TG,b_t}= *0.044* µmol gww hep^{-1}min^{-1}	Calculated from flux from FBA and steady state TG,b concentration
		K_{m,TG,b_t}=*0.4* µmol/gww hep	Set equal to steady state TG,b concentration (assumed)
$J_{ALA,b\text{-}t,net}$	$\frac{V_{max,ALA,b-t}(C_{ALA,b}-C_{ALA,t})}{(K_{m,ALA,b-t}+C_{ALA,b}+C_{ALA,t})}$	V_{max,ALA,b_t}=*12* µmol gww hep^{-1}min^{-1}	Calculated from in vivo flux and steady state ALA,b concentration
		K_{m,ALA,b_t}=*0.56* µmol/gww hep	Set equal to steady state ALA,b concentration
$J_{BHB,b\text{-}t,net}$	$\frac{V_{max,BHB,b-t}(C_{BHB,b}-C_{BHB,t})}{(K_{m,BHB,b-t}+C_{BHB,b}+C_{BHB,t})}$	V_{max,BHB,b_t}= *2.64* µmol gww hep^{-1}min^{-1}	Calculated from in vivo flux and steady state BHB,b concentration
		K_{m,BHB,b_t}=*0.85* µmol/gww hep	Set equal to steady state BHB,b concentration
$J_{pyr,b\text{-}t,net}$	$\frac{V_{max,PYR,b-t}(C_{PYR,b}-C_{PYR,t})}{(K_{m,PYR,b-t}+C_{PYR,b}+C_{PYR,t})}$	V_{max,PYR,b_t}=*8* µmol gww hep^{-1}min^{-1}	Calculated from in vivo flux and steady state PYR,b concentration
		K_{m,PYR,b_t}=*0.062* µmol/gww hep	Set equal to steady state PYR,b[15] concentration
$J_{AcAc,b\text{-}t,net}$	$\frac{V_{max,AcAc,b-t}(C_{AcAc,b}-C_{AcAc,t})}{(K_{m,AcAc,b-t}+C_{AcAc,b}+C_{AcAc,t})}$	$V_{max,AcAc,b\_t}$= *34.8125* µmol gww hep^{-1}min^{-1}	Calculated from in vivo flux and steady state AcAc,b concentration
		$K_{m,AcAc,b\_t}$=*0.7* µmol/gww hep	Set equal to steady state AcAc,b concentration

Table 2. Steady state results, at the overnight fasted state, experimental and calculated, with upstream blood concentrations given here: C^*_{Glc}= 4.6 mM; C^*_{LAC}=1.7 mM ; C^*_{PYR}=0.12mM; C^*_{FFA}=1.5 mM; C^*_{AcAc}=0.43 mM; C^*_{BHB}= 1.2 mM; F_{blood} =6.57 ml/min ; V_{tissue}=*5.25 cm;* V_{blood} *=1.03* cm^3 . Reaction rates (R_i) and transport rates ($J_{i,b\text{-}t}$) are given in Table 1 (+: production rate, -: uptake rate). For details please refer Chalhoub et al. (2007)

Metabolite Concentrations μmol gww hep^{-1}			**Fluxes** μmol gww $hep^{-1}min^{-1}$		
	Calculated	**Experimental**		**Calculated**	**Experimental**
Glc,tissue	6.3	4.5-6	$J_{GLC,b\text{-}t,net}$	1.11	1.2-1.9
Glc,blood	5.55	5.07-5.48	$J_{LAC,b\text{-}t,net}$	-1.38	-1.54
F6P	0.039	0.046	$J_{BHB,b\text{-}t,net}$	1.09	0.93
F1,6BP	0.0023	0.016	$J_{ALA,b\text{-}t,net}$	-0.59	-0.64
G6P	0.087	0.102	$J_{PYR,b\text{-}t,net}$	-0.12	-0.14
glycogen	109	109-175	$J_{FFA,b\text{-}t,net}$	-0.87	-0.8
GAP	0.015	0.021	$J_{GLR,b\text{-}t,net}$	-0.96	-0.14
GR3P	0.25	0.31	GK	0.57	
PEP	0.0061	0.05	G6Pase	1.68	
PYR,blood	0.024	0.062	GI	1.07	
PYR,tissue	0.023	0.059	GAP→F1,6BP	2.15	
LAC,blood	0.59	0.85-1.2	FBPase	1.08	
LAC,tissue	0.46	0.35-0.95	PFK	0.007	
AcAc,blood	1.47	0.68-0.99	PEP→GAP	2.08	
AcAc,tissue	1.61	0.5-0.78	PK	0.0003	5.56
BHB,blood	2.07	0.85-1.7	PYR→PEP	2.09	3-3.6, 7.9
BHB,tissue	5.6	2.23	LDH	1.26	
ALA,blood	0.23	0.5	GLR→GR3P	0.099	
ALA,tissue	0.18	0.47	GR3P→GAP	0.06	
AcCoA	0.13	0.13	FAT_syn	0.71	
ATP	3.46	3.43	FFA→AcCoA	0.86	
ATP+ADP+AMP	5.07	3.68-5.2	TG_f	0.11	
$NADH(m)/NAD(m)^+$	0.25	0.18	AcCoa→AcAc	4.83	
$NADH(c)/NAD(c)^+$	0.0021	0 .0017	OxPhos	8.20	
			TCA	1.37	1.7
			$J_{TG,b\text{-}t,net}$	0.03	
			PDC	0.0023	

Table 3. Initial conditions and input functions used in simulation of the perfused liver. ($R_{FA\text{-}endo}$=rate of endogenous fatty acid oxidation, normalized to µmol C_{16} (palmitate); $J_{FA\text{-}b\text{-}t}$ = the sum of the uptake rate of FFA and rate of endogenous fatty acid oxidation). For details please refer Chalhoub et al. (2007)

Lactate perfusion	Initial conditions used in Eqn. 4	Saline pre-perfusion; $0 < t \leq 30$	Lactate infusion; $30 < t \leq 60$	Lactate + FA; $60 < t \leq 90$
	$C_{i,perfusate}$ (t=0) =0; *i*=Glc, LAC, BHB, AcAc (saline pre-perfusion contains no substrate)	$R_{FA\text{-}endo}$ = 0.105 µmol gww $hep^{-1}min^{-1}$, assumed to be equal to experimental measurements of ketone production during this period[65].	$R_{FA\text{-}endo}$ = 0.0573 µmol gww $hep^{-1}min^{-1}$, as estimated[65] from ketone production. $C_{LAC,,perfusate}$ = 10(1-exp(-(t-30)/τ) mM (constant LAC concentration of 10 mM in perfusate); τ is time constant for achieving change in susbstrate concentration, set to 4 min.	$J^{*}_{FA\text{-}b\text{-}t}$= 0.0573+0.27(1-exp(-(t-60) /τ), τ=2.5 min; total rate of 0.33 µmol gww $hep^{-1}min^{-1}$ determined from experimental measurements of oleate infusion[65]. $C_{LAC,,perfusate}$ =10 mM
Pyruvate perfusion	Initial conditions used in Eqn. 4	Saline pre-perfusion; $0 < t \leq 30$	Pyruvate infusion; $30 < t \leq 90$	Pyruvate + FA; $90 < t \leq 120$
	$C_{i,perfusate}$ (t=0) =0; *i*=Glc, LAC, BHB, AcAc, PYR (saline pre-perfusion contains no substrate)	$R_{FA\text{-}endo}$ = 0.105 µmol gww $hep^{-1}min^{-1}$	$R_{FA\text{-}endo}$ =0.0573 µmol gww $hep^{-1}min^{-1}$ $C_{PYR,,perfusate}$ = 2(1-exp(-(t-30)/ τ) mM (constant PYR concentration of 2 mM in perfusate); τ=3 min. $C_{LAC,,perfusate}$ calculated from Eqn. 3.	$J^{*}_{FA\text{-}b\text{-}t}$ = 0.0573+0.27(1-exp(-(t-60) / τ), τ=2.5 min; experimental FA uptake not reported; assumed equal to data from lactate perfusion. $C_{PYR,,perfusate}$ =2 mM